NTNU

Norwegian University of
Science and Technology

Control of Wave Energy Converter with constrained electric Power Take Off

Eiril Bjørnstad

Master of Science in Energy and Environment
Submission date: January 2011
Supervisor: Marta Molinas, ELKRAFT

Norwegian University of Science and Technology
Department of Electric Power Engineering

Problem Description

The work in the Thesis will consist on the implementation of control strategies for improving the power extraction from the sea waves through a wave energy converter composed of a point absorber in heave directly connected to an entirely electric power take off system. The power take off system will be composed of an electric generator, and a back to back converter which will be connected to a fictitious grid that will be defined during the course of the work. The main focus will be on the practical implementation of the well known control techniques for wave energy extraction and based on that, modification of the techniques will be suggested in order to identify a viable solution that will respect rating constraints and energy storage requirements. Analytical calculations and simulations will be the basic tools used for carrying out the work.

Assignment given: 06. August 2010
Supervisor: Marta Molinas, ELKRAFT

Abstract

Because of ocean waves' high energy density and substantial, global technical potential wave energy might become a significant contributor to supply the world's increasing energy demand. The nature of ocean waves is strongly irregular and the power generation from a Wave Energy Converter will have large fluctuations what is a challenge for the electrical system. In the history of wave energy research the focus has been on controlling devices for increasing the absorbed power based on results from mechanical and hydrodynamic mathematical analysis. However, recent work shows that the peak of produced power increases compared to the average absorbed power when traditional control strategies like passive loading and optimal control are applied. The rating and the energy storage requirements of the electrical system will then be increased and the gain due to the increased power production might be lost.

In recent work a control strategy that optimizes the torque of the generator with respect to a power saturation level is presented. The work in this report focuses on a practical implementation of this strategy. Further, modifications to meet the torque and speed limitations of the system are made. A control algorithm is presented that utilizes the overrated speed region of the generator to maximize the power production with regards to the power and torque ratings. Simulations for irregular waves and control parameters chosen according to passive loading are then executed and the control algorithm is realized by use of field oriented control of the induction generator. The average absorbed power is changed only to moderate extends compared to the unconstrained case. At the same time the peak to average ratio and the maximum torque is considerably reduced. However, the strategy's reduced torque capability results in a higher maximum speed and pull out speed can be reached. Consequently there will be a trade off between investment costs, produced power and operation range of the system. Therefore the system should be optimized with respect to torque and power limitations, costs, produced power and pullout speed.

Preface

This thesis is the final work in my degree in Master of Technology in electric power engineering at Norwegian University of Science and Technology.

I would like to thank my supervisor prof. Marta Molinas at the Department of Electrical Power Engineering, who has guided me and been accessible when I needed some help to move on with my work. Thanks to my co-supervisor post doc. Elisabetta Tedeschi, for providing me literature. I also like to thank the Wave Energy Project at Fred Olsen Ltd for providing me with measurements, and a special thanks to Jonas Sjolte Bakken for his views and for the good conversations.

The working-days would not have been the same without my fellow students, and I would like to thank them for all their support and for the coffee breaks. Finally, I would like to thank for the backup I have received from my family and my lifepartner.

Contents

List of Figures

List of Tables

Chapter 1

Introduction

1.1 Background

The oil crisis in 1973 highlighted the vulnerability in the world's energy utilisation pattern and the interest in renewable energy resources as wave energy for electric power generation grew. The last years focus on increasing energy consumption, demand for sustainable development and oil shortage in the future have additionally lead to an growth in supporting policies from the world's governments, and the number of RD&D projects in ocean energy has increased in the 21st century[3]. The average energy intensity of ocean waves are higher than for solar and wind energy[4], and with a world potential in the same range as the total electricity consumption in the world[5] wave energy has potential of being a significant contributor to reach worlds energy demand.

Wave energy technolgy are however less mature than wind technology, and most wave energy devices are in the intermediate stage of development[6, 7]. Ocean waves are strongly irregular both in amplitude and frequency, and a Wave Energy Converter (WEC) has to convert the slow irregular motion of the wave into high quality electric power that satisfy grid requirements at a competitive price. There exist a wide range of different device concepts amoung the wave energy converters that are currently under development, and the pursued conversion principles in the devices consist of different types of absorbers and force reactions, exploits different modes of motion and some use techonlogy based on working fluids while others have a all electric power take off.[8, 3] This big variation in the applied technologies illustrates the need for more research to identify optimum solutions, and the difficulty of concluding on the

most suitable systems are pointed out to be one of the main barriers of the field by IEA's Implementing Agreement on Ocean Energy Systems.(iea)

The work presented in this report focus on modifications of well knowned control teqnuiques for a point absorber decive with all electricpower take off. The utilization factor of a point absorber can be increased by controlling its natural frequency at different sea states and realization of the theoretical maximum power that can be produced have recieved a lot of attention during the history of wave power development.[9, 10] The control problem span across several different special fields like statistics, hydrodynamics, mechanical engineering and electrical power engineering, and considering the irregular nature of the waves the complexity of the control algorithms often get high. The approch in the performed research in the past has mainly been from an hydrodanamic and mechanical point of view, but recent work performed in [11, 12, 13] shows that the optimal control strategy for the systems is strongly dependent on the limitations of the electric power take off. Based on the work that have been performed so far and practical implementation of these strategies a control algorithm that consider rating constrains of both power and torque of the electric system is developed. The objective is to identify a viable solution for control of point absorber that respect the constrains of the electric system as a step in developing reliable and cost-efficient power plants.

1.2 The investigated system and control strategies

Figure 1.1 shows the topology of the investigated system which consist of a spherical point absorber device connected to the generator shaft by a gear that consist of linear to rotational gear and then a rotational to rotational gear. The all electric Power Take Off have a back to back converter and an induction generator, and the proposed control strategy is realized by vector control and carrier based PWM modulation. The complexity of the system is high and simplifications that make it possible to model the system without loss of the general behavior of a point absorber device for irregular waves are made. Chapter 2 gives a simplified mathematical model of the hydrodynamic and mechanical system as well as a short introduction to well known control strategies. Chapter 3 treats the electrical system and the constrains due to the rating and energy storage requirements and at the end of the chapter the proposed control strategy is presented. A simulation model in Matlab/Simulink is built to investigate the performance of the proposed control strategy for irregular waves and passive loading for the proposed control strategy.

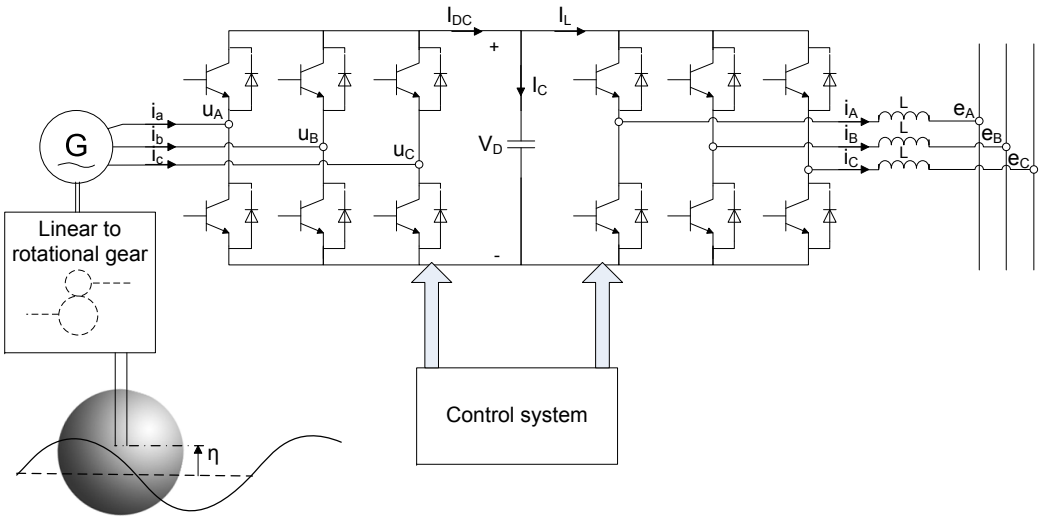

Figure 1.1: System topology of the investigated system

Chapter 2

Modelling and control

There exist a large number of different design concepts for extracting power from ocean waves and the development of these devices is at too early stage to conclude on an optimum solution. The most common technology among WEC's that are currently in development is the point absorber which is a floating device that can absorb energy from incoming waves independently of the direction of the waves. [14] The work in this report will focus on a spherical point absorber device, but the results of the analysis will indicate some tendencies of the behavior of point absorbers of different geometry or other oscillating wave energy converters. This chapter will provide a simplified mathematical model of the ocean waves and the motion of the buoy, and finally an introduction to well known control strategies to improve the power extraction.

2.1 The Wave resource

To model the interaction between the point absorber and the ocean waves a describtion of the sea surface motion must be proceeded. By applying linear theory ocean waves can be described as the superposition of a large number of harmonic waves where each wave component has different amplitude, phase, period and direction as illustrated in figure 2.1.[15]

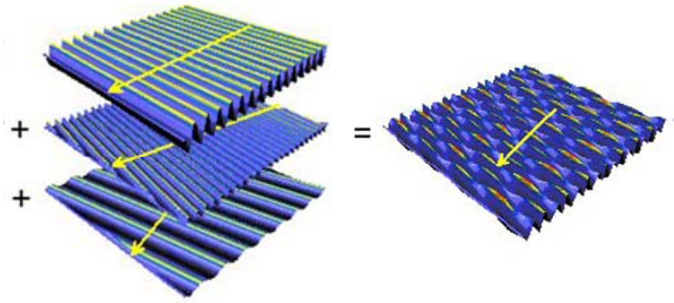

Figure 2.1: Variation in direction, frequency and amplitude of real sea waves[1]

A variance density spectrum provides a statistical representation of the surface elevation ζ of the ocean waves and the variance density spectrum S as function of frequency or radian frequency is given by the defenition in equation 2.1.[15, 16] The underbar indicates that the elevation ζ is a random variable and the overbar denotes the time average.Consequently the spectrum gives the distrubution of the variance of the sea-surface elevation over frequencies or radian frequencies, and it has untis $\left[m^2/Hz\right]$or $\left[m^2s/rad\right]$ respectively.[15] Stored energy per unit surface is given by equation 2.2[16]. From this relation it is clear that the variance density spectrum is equivalent to an energy spectrum of the described sea state.

$$\overline{\underline{\zeta}^2} = \int_0^\infty S(f)\,df = \int_0^\infty S(\omega)\,d\omega \tag{2.1}$$

$$E = \rho g \overline{\underline{\zeta}^2} = \rho g \int_0^\infty S(f)\,df \tag{2.2}$$

A statistical stationary sea state at a one geographic location can be described by different average wave parameters, and the number of parameter input a model has will decide the accuracy of the resultant characteristic.[15] However, statistically data can be difficult to obtain and the equations of motions will be of a high order. In this report the variance in direction of the waves is neglected to simplify the model. Under the assumption of such plane progressive waves on deep water or at finite but constant depth, only a one dimensional variance density spectrum is required to make the two dimensional description of the surface elevation (in x-direction and time), and Bretschneider (1959), Pierson-Moskowitz (1964), and Jonswap (1973) are some of the spectrums that are most commonly used.[17] Different wave conditions due to geographical location and maturity of the development of the sea state

will affect which spectrum should be applied [15], but for the work in this report the irregular behavior of the waves are the most interesting aspect. A modified Pierson-Moskowitz spectrum recommended by the International Ship and Offshore Structures Congress referred to as the ISSC-spectrum is therefore applied, which is a spectrum for a fully developed sea [1][19, 17] The ISSC spectrum is defined by equation 2.3, where $H_{1/3}$ is the significant wave height defined as the mean of the highest one-third of the waves and T_1 the mean wave period or the characteristic period. [17]

$$\frac{S(\omega)}{H_{1/3}^2 T_1} = \frac{0.11}{2\pi}\left(\frac{\omega T_1}{2\pi}\right)^{-5} exp\left[-0.44\left(\frac{\omega T_1}{2\pi}\right)^{-4}\right] \tag{2.3}$$

A discrete spectrum $S(\omega_k)$ with N wave frequency components ω_k can be calculated based on equation 2.3, with randomly generated phase ϕ_k and frequency components randomly chosen in each interval. The times series of the wave elevation can then be calculated from equation 2.4 where k denotes the number of the angular frequency component. [8]

$$\zeta(t) = \sum_{k}^{N} \Re\left\{\sqrt{2\Delta\omega S(\omega_k)} e^{i\omega_k t + \phi_k}\right\} \tag{2.4}$$

It can be useful to relate the mean wave period T_1 to other commonly used period parameters that are either easier to determine experimentally or to compare the spectrum to other spectrum or single harmonic waves. Table 2.1 provides the definition of several common parameters and the ratio between them that are valid for spectrums on the form of equation 2.3 amoung others; see [19] for derivation.

Period	Definition	K,$K = {}^{T_i}/_{T_o}$
Modal period T_o	Reciprocal of the peak frequency	1
True average period or energy period T_e	The true average period of the elements of the wave	0.857
Charactersitic period or mean wave period T_1	Reciprocal of the true average frequency	0.772
Zero-upcrossing periodT_z	The average period of zero upcrossings in the wave record	0.710
Significant period T_s	Average of the 1/3 highest wave in the record	0.946

Table 2.1: Ratio between several common definitions of wave period

[1] A fully developed sea exists if the wind has blown for a long time over a sufficient distance. Areas as the North sea, the eastern pacific ocean and the Gulf of Mexico is characterized as ocean areas that in most case only have partially developed seas(simplifed) The Jonswap spectrum is then to prefer [18]

The total transport of energy per unit width J (also refered to as the wave-power level) of the wave front for a single progressive, plane and harmonic wave with apmlitude A and period T are given by equation 2.5 and for real ocean waves by equation 2.6, where ρ is the water density, g the acceleration of gravity and $c_g(f) = {}^{gT}/_{4\pi} =$ the group velocity of the waves [14]

$$J = c_g E = c_g \frac{\rho g}{2} |A|^2 \tag{2.5}$$

$$J = \rho g \int_0^\infty c_g(f) S(f)\, df = \frac{\rho g^2}{64\pi} T_e H_{1/3}^2 \tag{2.6}$$

To make a good as possible basis to compare the analysis done with regular and irregular waves the amplitude of the harmonic wave in the regular case should be chosen as $\frac{1}{2\sqrt{2}} H_{1/3}$ and the period equal to the energy period of the spectrum of the irregular sea state, which leads to the same wave-power level for the two cases.

2.2 The Equation of motion

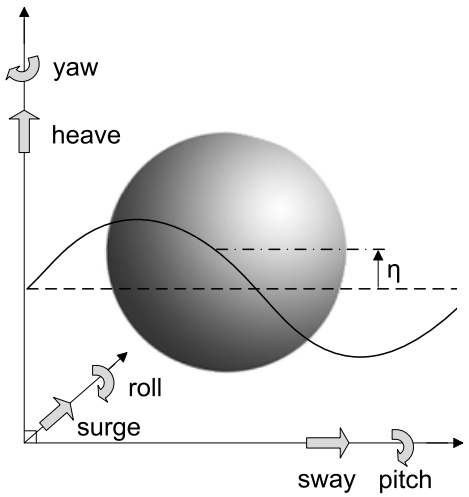

Figure 2.2: Degrees of freedom of the motion of a point absorber

A floating rigid body like the point absorber has six degrees of freedom; three translational and three rotational as showed in figure 2.2. [15] To reduce the complexity of the model

of the point absorber in figure 2.2 only movement in heave is considered. Newton's second law of motion then reduces to a first order equation given by 2.7, where f_e is the excitation force, f_r the radiation force,f_s the hydrostatic stiffness, f_m the machinery force, f_v the viscous damping , f_l the mooring forces, f_o environmental forces, u the speed of the bouy in heave and $M = m+J_{eq}g_r^2$ the sum of the mass of the buoy and added mass due to the total inertia of the power take off. [8] J_{eq} is the total inertia referred to the generator side and consequently g_r is the gear ratio between the generator shaft and the linear buoy motion in heave.

$$M\dot{u} = f_e + f_r + f_s + f_m + f_v + f_l + f_o \tag{2.7}$$

The viscous damping, mooring forces and environmental forces has not been included in this work; more about modeling of these forces can be found in literature, e.g. [8]. The machinery force is provided by the power take of system, which in this case consist of an all electric power take off with an induction generator and a back to back converter, and is treated in detail in chapter 3.

2.2.1 The Hydrodynamic forces acting on a point absorber in heave

An approximation of the hydrodynamic forces is implemented by use of linear wave theory, which is a valid simplification for waves that have a small amplitude compared to the wave length and the water depth, and are located at deep or finite water depth so the influence of the seabed can either be neglected or taken into account without a large increase of complexity.[15] Consequently, the extreme-wave situations are not taken into account, but during such conditions the WEC most likely has to stop producing. To apply linear wave theory the water must additionally be assumed to behave as an irrotational ideal fluid with no viscosity, a constant density and to be incompressible.[15] Under these assumptions the harmonic waves do not influence each other and the radiation and excitation parameters can be calculated for each harmonic wave, and the principle of superposition can be used to calculate the total forces. The hydrodynamic parameters can be calculated based on the velocity potential function, which can be obtained by linear theory by solving the Laplace equation combined with a set of boundary conditions. [15]

Hydrostatic force

The hydrodynamic force is the sum of a buoyancy force due to displaced water and the gravity force on the body and can for small heave excursions be modeled as the product of

the deviation η from the equilibrium position and the hydrostatic stiffness S at equilibrium as in equation 2.8, where A_w is the water plane surface area of the body. [8]

$$\hat{F}_s = -S\eta = -\rho g A_w \eta \tag{2.8}$$

Excitation force

A fixed body exposed to an incoming wave will experience a force due to the undisturbed incident wave and the diffracted wave that is created as a result of the interaction between the wave and the fixed body which is named the excitation force.[16]The excitation force is non causal and can be related to the wave elevation ζ by equation 2.9 where $\hat{H}_{F\zeta}(\omega)$ is the excitation force coefficient(the uppercase indicates complex values). [8]

$$\hat{F}_e(\omega) = \hat{H_{F\zeta}}(\omega)\hat{\zeta}(\omega) \tag{2.9}$$

There exist several methods to obtain the excitation force for time domain simulations, either by real time estimation or pre-calculation of the time series. The force can for instance be pre-calculated in the time-domain by calculation of an excitation force spectrum $S_{F,k}$ from the hydrodynamic parameter $\hat{H_{F\zeta}}$ and the discrete variance density spectrum $S(\omega_k) = S_k e^{j\phi_k}$, as shown in 2.10 and 2.11.[8]

$$S_{F,k} = \left|\hat{H}_{F\zeta,k}\right|^2 S_k \tag{2.10}$$

$$\phi_{F,k} = \angle \hat{H}_{F\zeta,k} \tag{2.11}$$

The excitation force given in complex form for frequency component k is then given by 2.12. The total excitation force from N frequency components are obtain by 2.13. [8]

$$\hat{F}_{e,k} = \sqrt{2S_{F,k}\Delta\omega}e^{(j\phi_k + \phi_{F,k})} \tag{2.12}$$

$$f_e(t) = \sum_{k=1}^{N} \Re\left\{\hat{F}_{e,k}e^{j\omega_k t}\right\} \tag{2.13}$$

Radiation force

A oscillating body in still water will create a radiated wave and the force on the body due to this wave is called the radiation force. [16] In the frequency domain the radiation force can be described by 2.14 where $m_r(\omega)$ is the added mass, $R_r(\omega)$ the radiation resistance and $\hat{u}(\omega)$ and $\hat{a}(\omega)$ the speed and the acceleration of the buoy. [8]

$$\hat{F}_r(\omega) = -m_r(\omega)\hat{a}(\omega) - R_r(\omega)\hat{u}(\omega) \tag{2.14}$$

The energy absorption of a point absorber device is caused by the radiated wave that interferes destructively with the incoming wave, so to absorb power from the ocean waves some of the incoming energy has to be radiated.[14]The radiated power is dependent of the radiation resistance[16], and consequently the device's hydrodynamic design is a very important factor to its absorption ability. The added mass, also referred to as the radiation reactance, is caused by the added stored energy of the water due to the motion of the buoy and the value is determined by the difference between the kinetic and potential added energy. [16]

In time domain the radiation force can be simplified to 2.15, where $m_r(\infty) = \lim_{\omega \to \infty} m_r(\omega)$ is the added mass at the limit of infinity frequency, $k(\omega) = \mathcal{F}\{k(t)\} = i\omega\{m_r(\omega) - m_r(\infty)\delta(\omega)\} + R_r(\omega)$ the integration kernel and η the position of the buoy in heave.[8]

$$f_r(t) = -m_r(\infty) - \int_0^t k(t-\tau)\dot{\eta}(\tau)d\tau \tag{2.15}$$

For a linear system a convolution term can be replaced by an ordinary differential equation or a state space representation without loss of accuracy, but since the hydrodynamic parameters in the integration kernel are frequency dependent and non-linearities in the equation of motion can occur (for instance due to a non-linear machinery force) an approximation of the convolution term has to be introduced. Approximating the radiation parameters by constants is a valid simplification for devices that are operating far from optimum oscillations so that the machinery damping is dominant compared to the radiation damping. The radiation force can then be expressed by2.16.[8]

$$f_r(t) = -m_r(\omega_k)\ddot{s}(t) - R_r(\omega_k)\dot{s}(t) \tag{2.16}$$

However, close to optimum the convolution integral should be modeled more accurately, for

instance by a state space model approximation as equation 2.18. An different identification methods for $\mathbf{A}_k$, $B_k$and $\mathbf{C}_k$ from the hydrodynamic parameters can be found in [20].

$$\dot{\mathbf{z}}(\mathrm{t}) = \mathbf{A}_\mathrm{k}\mathbf{z}(\mathrm{t}) + \mathrm{B}_\mathrm{k}u(t) \tag{2.17}$$

$$f_r(t) = -\mathbf{C}_k\mathbf{z}(t) \tag{2.18}$$

2.2.2 Electric analogue

Disregarding the mooring forces, viscous forces and environmental forces the equation of motion given in complex values, if the expressions for the hydrostatic stiffness and the radiation force from the last section is included, is reduced to 2.19 .

$$\left\{ i\omega(M + m_r(\omega)) + R_r(\omega) + \frac{S}{i\omega} \right\} \hat{u}(\omega) = \hat{f}_e(\omega) + \hat{f}_m(\omega) \tag{2.19}$$

To execute analytical calculations of the system an electric analogue will be used based on equation 2.19 as shown in figure 2.3, as applied in [16]. The speed of the buoy is then equivalent to the current of the electric circuit, the forces equivalent to voltages and the mechanical and hydrodynamic parameters M, m_r, R_r and S can be represented by an impedance $Z_b = R_r + \overbrace{i\omega(M + m_r(\omega)) - i\frac{S}{\omega}}^{iX_b} = R_b + i\omega L_b - i\frac{1}{C_b\omega}$.

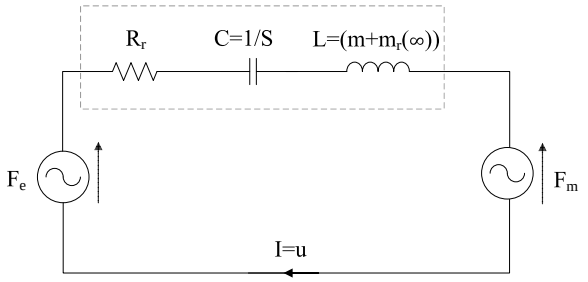

Figure 2.3: Electric analouge of the point absorber

By basic circuit theory it can be noticed that energy is dissipated due to the radiation resistance. Kinetic energy is saved in the inductance that represents the mass and added mass

of the buoy, and potential energy is saved in the capacitance equivalent to the hydrostatic stiffness when the buoy oscillates with a speed $\hat{u}(\omega)$. The power balance of the system can then be obtain by the circuit in figure 2.3 and are given in equation 2.20, where $\hat{S}_e$ is the power supplied by the excitation force, $\hat{P}_r$ the radiated power, $\hat{Q}_p$ and $\hat{Q}_k$ the reactive power due to change in potential and kinetic energy and $\hat{S}_m$ the apparent power absorbed by the power take off. From the equations it can easily been seen that to absorb power some active power must be radiated, as stated in section 2.2.1.

$$\hat{S}_e = \hat{F}_e\hat{u} = \hat{S}_m + \hat{P}_r + j(\hat{Q}_p + \hat{Q}_k) = \left\{-\hat{F}_m - \hat{F}_r + j(-F_s(t) - (M + m_r)\dot{\hat{u}})\right\}\hat{u} \tag{2.20}$$

The average excitation, radiation and machine active power assumed constant radiation resistance can be calculated by basic circuit theory to the expression given by 2.21-2.23, where γ_e is the angel between the speed phasor $\hat{u}$ and the excitation force phasor $\hat{F}_e$.

$$\overline{P}_e = \frac{1}{2}Re(\hat{S}_e) = \frac{1}{2}\left|\hat{F}_e\right|\left|\hat{u}\right|\cos(\gamma_e) \tag{2.21}$$

$$\overline{P}_r = \frac{1}{2}R_r\left|\hat{u}\right|^2 \tag{2.22}$$

$$\bar{P}_m = \overline{P}_e - \overline{P}_r = \frac{1}{2}(\left|\hat{F}_e\right|\left|\hat{u}\right|\cos(\gamma_e) - R_r\left|\hat{u}\right|^2) \tag{2.23}$$

Assuming a machinery force on the form $\hat{F}_m = -\hat{u}(R_m + jX_m) = -\hat{u}Z_m$ the average extracted active power by the power take off can be calculated from 2.24 to be:

$$\bar{P}_m = \frac{1}{2}\left|\hat{u}\right|^2 R_m = \frac{1}{2}\frac{\left|\hat{F}_e\right|^2 R_m}{(Rr + R_m)^2 + (\omega L_b - \frac{1}{\omega C_b} + X_m)^2} \tag{2.24}$$

2.3 Control

From equation 2.24 it is clear that the machinery force will affect the power production of the WEC and consequently the dynamic behavior of the buoy. An optimum oscillation with regard to power absorption occur when the speed u of the buoy has a optimum phase and amplitude compared to the excitation force, where the optimum amplitude condition is fulfilled when the

amplitude of the radiated wave is half the amplitude of the incident wave and the optimum phase condition is fulfilled when the speed is in phase with the excitation force.[21] This can be derived from equation 2.23, and mathematically it can be described by 2.25-2.27.

$$P_{m,max} = P_{r,opt} = \frac{1}{2} P_{e,opt} \tag{2.25}$$

$$|\hat{u}_{opt}| = \frac{1}{2} \frac{\left|\hat{F}_e\right|}{R_r} \tag{2.26}$$

$$\cos\gamma = 1 \tag{2.27}$$

For an oscillating system in one mode the optimum phase condition coincide with a resonance condition between the buoy and the incident wave.[21] To achieve both optimal amplitude and optimal phase condition it can be derived that the optimal machine force impedance $Z_{m.opt}$ has to be the complex-conjugated of Z_b.[8] This will lead to zero reactance in the total system and consequently will the excitation force and speed be in phase and the same solution as in 2.25-2.27 can be derived from equation 2.24. The optimum solution is non-causal, since the hydrodynamic parameters are anti-causal in the case of irregular waves [8], and different simplified control strategies has been introduced. A short introduction to different control strategies from literature are given below based on the work done in [8], while restrictions on the machinery force and the control strategy due to the power take off system are treated in chapter 3.

Passive loading

A machinery force on the form given by equation 2.28 is called passive or resistive loading, and have a pure resistive machinery force impedance.

$$F_m(t) = -R_m \dot{\eta}(t) \tag{2.28}$$

The optimal resistance when passive loading is applied can be derived by substituting eqation 2.24 into 2.24 and locating the maximum of the function, and are then found to be:

$$R_{m,opt}(\omega) = \sqrt{R_b^2(\omega) + X_b^2(\omega)} \tag{2.29}$$

Since the machinery force will be in phase with the velocity of the buoy there will be no reactive power flow in the power take of system, and the power flow will be unidirectional.

Approximate complex-conjugate control

Approximate complex-conjugate control is based on finding a causal approximation to the optimal force, for instance implementing constant hydrodynamic parameters corresponding to the values obtained for an angular frequency ω_k that can be optimized for each sea state. The machinery force in the time-domain is then given by 2.30.

$$F_m(t) = (M + m_r(\omega_k))\ddot{\eta}(t) - R_r(\omega_k)\dot{\eta}(t) + S\eta \tag{2.30}$$

Attention should be given to the stability margins when choosing the control parameters for the complex-conjugate control, as the system can get unstable. [8] Additionally will the control strategy, as opposed to passive loading, require bidirectional power flow and consequently must the generator operate as a motor in periods. [12]

Tracking of approximate velocity

The control based on tracking of approximate velocity tries to track the optimal velocity given by equation 2.26, and to achieve this an approximation of the radiation resistance $R_r(\omega)$ has to be made. A simple solution is to replace it with a constant resistance, which gives; $u_{ref} = \frac{F_e}{2R_r(\omega_k)}$, and a P or PI controller can be implemented to realize the tracking. [8]

Model-predictive control

The principle of model-predictive control is to optimize the performance of the system over a short period T_h by using a discrete-time model of WEC combined with a prediction of the excitation force. The optimization can for instance be carried out by solving a quadric programming optimization problem with respect to output power, and system constrains can be implemented in the optimization problem. [8]

Latching and Clutching

Phase control of the buoy can be executed by latching or clutching control, which both require some kind of mechanical mechanism to be implemented. Latching blocks the buoy from moving

in parts of the period to obtain optimal phase, while clutching control decouples and couples the machinery and in that way lets the buoy move freely in periods. In that way can optimal phase condition be obtained without reactive power flow in the machinery. The challenge with the control strategies is the predicting of the execution instants for a device in real irregular sea states that have several degrees of freedom.[8]

Chapter 3

Constrains of the electric system and the proposed control strategy

There exist several different power electronic interfaces and generator types that can be suitable for an all electric power take off for a wave energy converter. The machinery force needed for the control strategy will affect the specifications for the power electronic interface and to enable variable speed drive with bidirectional power flow a back to back converter is chosen. The requirements for a generator used in a wave energy converter differ from the ones the conventional generators are designed according to. The system performance can be improved by use of generators that are a specially designed to cope with the low speed irregular oscillating movement, the demand for a low maintenance level and the high peak forces. Linear permanent-magnet generator for use in WECs is an example of a field of research that has evolved as a consequence of this. However, there are still problems related to the use of such generators.[22] More research should be performed on several generator technologies to find suitable solutions, and a squirrel cage induction generator is used for the work in this report. The benefits of an induction machine are its low price and rugged construction[2] which suits the specifications for generators used in Wave Energy Converters. A linear to rotational gear has to be included when using a rotational generator in an all electric power take off, but due to the low efficiency of generators operated at low speed, as pointed out in [22], gears may turn out to be necessary to increase the speed.

The investigated topology with the induction generator in series with a full back to back voltage source converter is shown in figure 3.1. The DC link decouples the control of the two

converters; the generator side converter can provide magnetization of the induction generator and control of the electromagnetic torque while the grid side converter can control the power factor and the power flow.[23] Since there is no energy storage present in the system the grid side converter should control the power flow to maintain a constant DC link voltage. The constraints given by the energy storage requirements, the losses and the rating of the electric components for the control strategy for the generator side converter are treated in the sections below, before the mathematical model of the electrical system that are needed to implement the control strategy are presented. A short introduction to the voltage source converter and carrier based modulation is provided in appendix C At the end of the chapter the proposed control strategy for the WEC is then obtained.

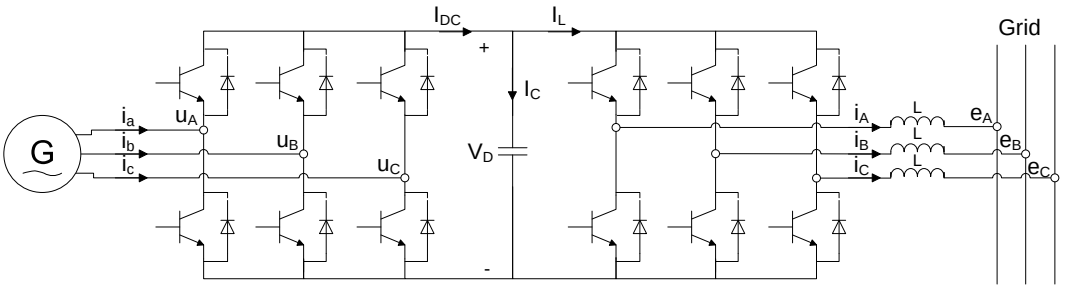

Figure 3.1: The system topology of the all electric Power Take Off

3.1 Energy storage requirements and rating constrains due to power fluctuations

Figure 3.2 shows a power measurement in pu from a Fred Olsen point absorber test rig with all electrical power take off and shows typical power fluctuations for wave energy converters under real sea conditions. The fluctuations introduce several problems to both the mechanical and the electrical system and are one of the main barriers to achieve a reliable and cost-efficient technology.

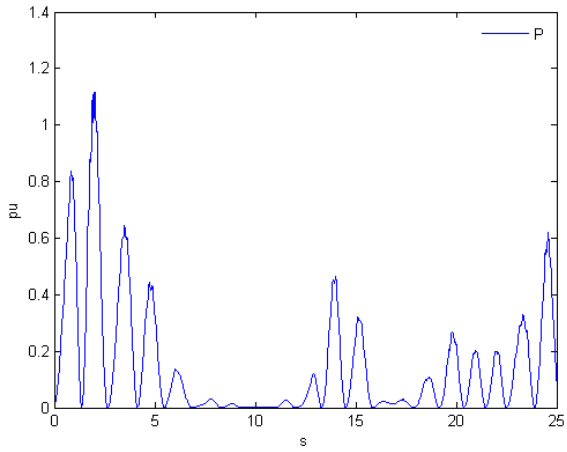

Figure 3.2: Scaled power measurements from Fred Olsen test rig

Energy storage requirements

In power system with a large amount of energy storage, as systems with a high share of hydropower and/or thermal power plants, the grid will behave as a stiff grid and the power system can receive fluctuating power without weaken the power quality significantly. But new challenges are introduced in obtaining safe, reliable and economic operation of power systems, because of the increasing number of distributed and renewable based generators [24] Therefore are distribution and grid codes specific for wind turbine generators introduced in addition to the general codes, and since the requirement for wave energy generators will probably be somewhat the same wave farms will have to operate more or less as conventional power plants[25]The large fluctuations in the incoming power can in the case of a weak grid influence the power quality of the grid, and if wave energy is going to represent a higher share in the power balance some kind of energy storage is needed to smooth the power fluctuations and provide the system with energy buffer for control of active and reactive power.

Rating constrains

The system must be designed to handle the peak forces, currents and voltages, and the fluctuating power leads to an overrating of the equipment compared to the mean power level. The weight and cost of the device will increase with the ratings and power smoothing at an early stage of the conversion chain would reduce the needed rating of the components.

Efficiency and power losses

The power losses of the components are for instance dependent of the load factor and the rating will therefore affect the efficiency of the electrical system. The efficiency of a two-level back to back voltage source converter will only decrease by a few percent at small loads [26], and an overrated VSC will mainly affect the investment costs and the weight as well as the harmonics in the three phase voltages due to the change in the amplitude modulation as shown in [2]. In an induction machine there will be stator and rotor copper losses, magnetic core losses, friction losses, windage losses and "stray load losses" due to the non-ideal behavior of the machine. [27] A typical shape of the efficiency curve for an induction generator for a specific ambient and machine reference temperature is shown in figure 3.3 and for light loading conditions the efficiency of the generator decrease dramatically.[27] During low production the magnetization current will be dominate compared to the produced current which explains the shape of the curve.

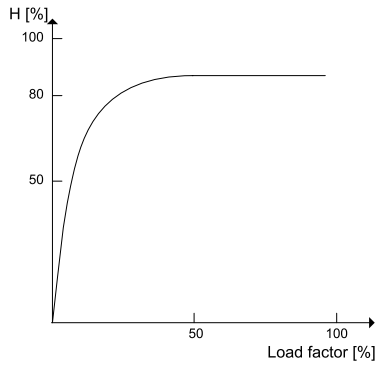

Figure 3.3: Efficiency of an induction generator as a function of the load factor

The copper losses and the core losses in an induction machine is given by equation 3.1 as a function of the stator resistance R_s, the rotor resistance R_r, the core loss resistanceR_m, the stator currents i_{sd} and i_{sq}, the rotor currents i_{rd} and i_{rq} and the core losses currents i_{sqa} and i_{sda}.[28]

$$P_{losses} = \frac{3}{2}\left[R_s(i_{sq}^2 + i_{sd}^2) + R_r(i_{rq}^2 + i_{rd}^2) + R_m(i_{sqa}^2 + i_{sda}^2)\right] \tag{3.1}$$

3.1.1 Calculations on the electrical analogue to evaluate the peak to average ratio

The control strategy of the generator will affect the peak to average ratio and the economical gain due to an increase in production can be lost because of the increase in the rating of the system and the required energy storage. [13] To analyze the peak to mean ratio analytically for a regular wave the electric analogue presented in chapter 2 can be applied.

The instantaneous active power absorbed by the power take off can be calculated by curcuit theory as follows:

$$
\begin{aligned}
P_m(t) = F_m(t)u(t) &= \left|\hat{F}_m\right| \cos(\omega t + \delta_{F_m}) \left|\hat{u}\right| \cos(\omega t + \delta_u) \\
&= \frac{\left|\hat{F}_e\right|\sqrt{R_m^2+X_m^2}}{\sqrt{(Rr+R_m)^2+(\omega L_b - \frac{1}{\omega C_b}+X_m)}} \cos(\omega t + \delta_{F_m}) \frac{\left|\hat{F}_e\right|}{\sqrt{(Rr+R_m)^2+(\omega L_b - \frac{1}{\omega C_b}+X_m)}} \cos(\omega t + \delta_u) \\
&= \frac{\left|\hat{F}_e\right|^2\sqrt{R_m^2+X_m^2}}{(Rr+R_m)^2+(\omega L_b - \frac{1}{\omega C_b}+X_m)} \overbrace{\frac{1}{2}\left[\cos\varphi_m(1+\cos 2(\omega t + \delta_{F_m})) + \sin\varphi_m \sin 2(\omega t + \delta_{F_m})\right]}^{\cos(\omega t+\delta_{F_m})\cos(\omega t+\delta_u)} \\
&= \bar{P}_m \left[(1+\cos 2(\omega t + \delta_{F_m})) + \tan\varphi_m \sin 2(\omega t + \delta_{F_m})\right]
\end{aligned}
\tag{3.2}
$$

where $\varphi_m = \delta_{F_m} - \delta_u$ is the power factor of the power take off defined by:

$$
\cos\varphi_m = \cos\left(\tan^{-1}\left(\frac{X_m}{R_m}\right)\right) \tag{3.3}
$$

By setting the first derivative of the power equal to zero the theoretical maximum power can be found to occur at $\omega t = \varphi_m/2 - \delta_{F_m}$, and the maximum power as a function of the mean power and the load factor is then obtained by equation 3.4.

$$
\widehat{P}_m = \overline{P}_m(1 + \frac{1}{\cos\varphi_m}) \tag{3.4}
$$

The impact of the control parameters on the average and peak absorbed power can then be analyzed for a specific regular wave based on equation 3.2-3.4, and figure 3.4-3.5 shows the peak and average power as a function of the control parameters for a regular wave with $A = 0.5$m and $T_s = 6$s for the investigated device of this work.

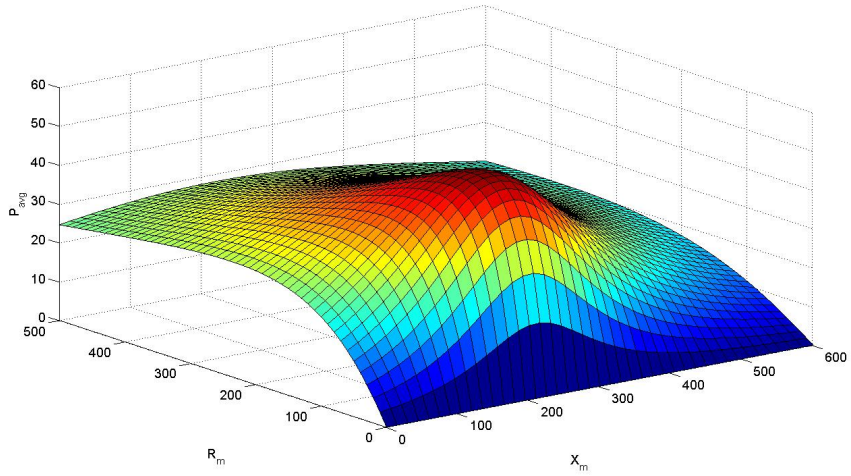

Figure 3.4: The average absorbed power as a function of the control parameters

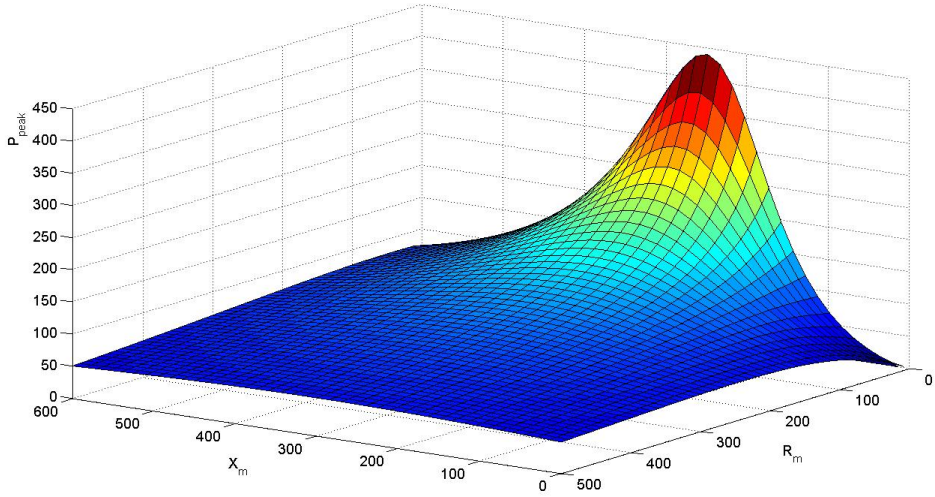

Figure 3.5: The peak power as a function of the control parameters

The maximum extracted power that occur at optimal phase and amplitude of the machinery force can be read from figure 3.4 to be 52.7 kW and require a machinery damping resistance of 93.38 kohm and a machinery reactance of $312,7$ kohm. From figure 3.5 it is evident that the peak power rises in the area around the optimal control parameters. The peak to average ratio for the maximum power absorption can be calculated to 4.5, but in the case of pure passive damping, which corresponds to a unity load factor, it will be reduced to the theoretical minimal value of 2. The results of the work performed in [12] [11] show that the peak to average ratio increase considerably when irregular waves are implemented, and use of optimal control will consequently require a significantly over rating of the electrical system.

Figure 3.6 shows the peak to average ratio as function of the load factor and shows how the ratio increase when a reactance are introduced in the machinery force. The load factor of 0.39 correspond to optimal control for the system for the chosen harmonic wave. The blue marker gives the load factor at optimal control of a different design which has a smaller reactance for the frequency used in this example, caused for instance by a different gemometrical shape of the WEC or a different gear ratio. The smaller reactance leads to a smaller load factor and consequentley also a smaller peak to average ratio.

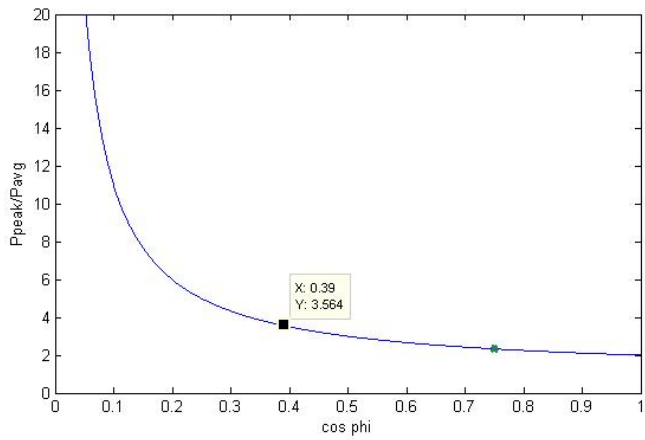

Figure 3.6: Peak to average ratio as a function of the power factor for the Power Take Off

3.2 Model and Control of Induction generator

3.2.1 Generator model in dq reference frame

The electrical rotor speed $\omega_m = {}^{p}/_{2}\omega_{mech}$ in electrical radians per second can be expressed by the angular speed of the dq reference frame ω_d and the angular speed with respect to the rotor A-axis ω_{da}, as shown in equation 3.5. [29]

$$\omega_m = \omega_d - \omega_{da} \tag{3.5}$$

If the induction machine is impressed the terminal voltages U_{sd} and U_{sq} the voltages, currents and fluxes of the machine in the dq reference frame are given by equation 3.6-3.10, where R_s and R_r are the stator and rotor resistances, L_s and L_r the stator and rotor inductances and L_m the per phase magnetizing inductance.[29] Notice that the rotor voltages are zero since the windings in the rotor are short-circuited in a squirrel cage machine.

$$U_{sd} = R_s i_{sd} - \omega_d \lambda_{sq} + \frac{d}{dt}\lambda_{sd} \tag{3.6}$$

$$U_{sq} = R_s i_{sq} + \omega_d \lambda_{sd} + \frac{d}{dt}\lambda_{sq} \tag{3.7}$$

$$\overbrace{U_{rd}}^{=0} = R_r i_{rd} - \omega_{da} \lambda_{rq} + \frac{d}{dt}\lambda_{rd} \tag{3.8}$$

$$\overbrace{U_{rq}}^{=0} = R_r i_{rq} + \omega_{da} \lambda_{rd} + \frac{d}{dt}\lambda_{rq} \tag{3.9}$$

$$\begin{bmatrix} \lambda_{sd} \\ \lambda_{sq} \\ \lambda_{rd} \\ \lambda_{sq} \end{bmatrix} = \begin{bmatrix} L_s & 0 & L_m & 0 \\ 0 & L_s & 0 & L_m \\ L_m & 0 & L_r & 0 \\ 0 & L_m & 0 & L_r \end{bmatrix} \begin{bmatrix} i_{sd} \\ i_{sq} \\ i_{rd} \\ i_{rq} \end{bmatrix} \tag{3.10}$$

The total electromagnetic torque of the machine in terms of the inductances and currents can be calculated from equation 3.11.[29]

$$T_{em} = \frac{p}{2} L_m (i_{sq} i_{rd} - i_{sd} i_{rq}) \tag{3.11}$$

Based on the equations given above the dynamical behavior of the induction generator can be modeled, where the speed ω_{mech} is an input from the mechanical system and the voltages from the voltage source converter. Temperature variations of the machine parameters, the core losses resistance and saturation effects are neglected and the errors because of this simplification must be considered. The most temperature dependent parameter is the rotor resistance, which can lead to deviation in the calculated fluxes. [27]

Flux weakning

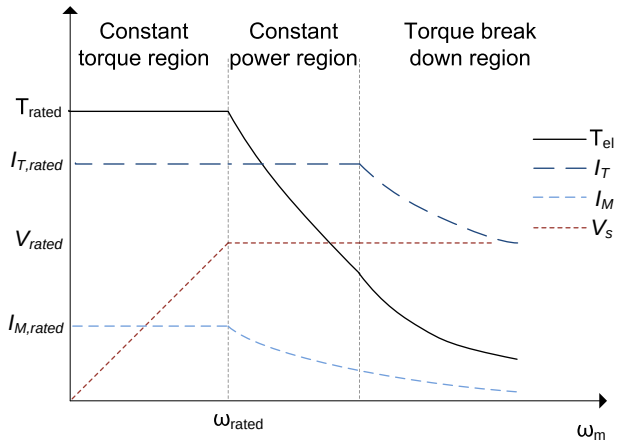

Figure 3.7: Characteristic and torque capability of an induction machine

By operating the induction generator at over rated speed the rating of the generator can be reduced to increase the utilization of the generator and to bring down the investment costs. The characteristic of the generator operating at over speed are analyzed below. The operation of an induction machine with constant rated torque up to rated speed are given in figure 3.7 and the operation can be divided into three regions.[30] Below rated speed the available torque is restricted by the current rating of the machine, while the stator voltage is below its rated value and increases with the speed. Parts of the stator current are used to produce the flux, as shown in the next secton, and the magnetization current I_M is kept constant in the first region to provide a constant flux.

When the machine reaches rated speed the stator voltage has increased to its rated value, as seen from figure 3.7, and a further increase in speed without any actions would lead to a stator voltage over its rated value. Introducing the leaking factor $\sigma = 1 - \frac{L_m^2}{L_r L_s}$ the per phase equivalent circuit for the induction generator in steady state with all the leakage inductance referred to the stator side are given by figure 3.8, and a phase diagram with values typical for the constant power region is given by 3.9.[30] From the phasor diagram it is clear that the voltage drop across $j\omega_e L_m^2/L_r$ is dominant and decreasing the magnification current will efficiently decrease the stator voltage and enable a further increase in speed without violating the current and voltage ratings. The torque of the machine is given by $T_e = K\,|\mathbf{I}_M|\,|\mathbf{I}_T|$ and a reduction in the magnetization current reduces the torque, and the machine cannot operate at rated torque above rated speed. When the voltage drop across $j\omega_e L_m^2/L_r$ is not dominant anymore $\mathbf{I}_s$ must be decreased to enable an increase in speed and the machine enters the torque break down region. Depending on the generator design this region normaly starts around 1.5-2 times rated speed. [2]

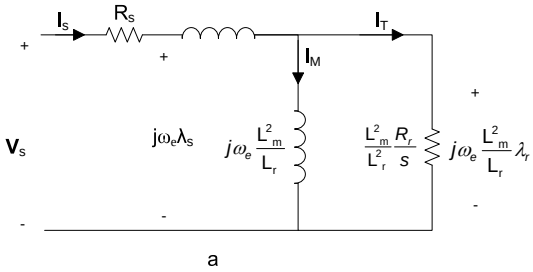

Figure 3.8: Equivalent diagram of the induction machine

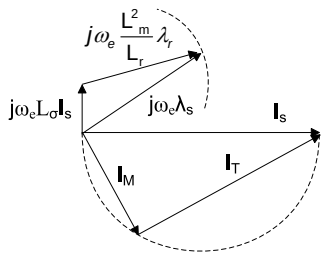

Figure 3.9: Phasor diagram during operation in constant power region

A common way to determine the flux reference above rated speed is to set the reference proportional to $1/\omega_r$[30] and the expression for the flux and torque reference is then given by 3.12 and 3.13. However, it should be noticed that this method may not utilize the total torque capability of the machine. From the phasor diagram in 3.9 it can be seen that when $\mathbf{I}_M$ are decreased $\mathbf{I}_T$ can be increased to some extend without exceeding the rating of Is.

$$T_{e,ref} = \frac{T_{e,rated}\omega_{m,rated}}{\omega_m} \tag{3.12}$$

$$\lambda_{r,rated} = \frac{\lambda_{r,rated}\omega_{m,rated}}{\omega_m} \tag{3.13}$$

3.2.2 Vector control of an induction generator

Vector control or field oriented control is a control technique that is based on inner current control loops in the dq-reference frame, and with the d-axis aligned along the rotor flux the d- and q-axis are approximately decoupled, and the flux and torque can be controlled independently. [29] ω_d is then equal to the synchronous speed, and ω_{da} equal to the slip speed. The equations for the slip speed, electromagnetic torque and the rotor flux can then be simplified to 3.14-3.16, and assuming constant parameters and while keeping the rotor flux constant a linear relationship between the q-axis stator current and the electromagnetic torque is obtained.

$$\omega_{da} = \frac{L_m}{\tau_r \lambda_{rd}} i_{sq} \tag{3.14}$$

$$T_{em} = \frac{p}{2} \lambda_{rd} \frac{L_m}{L_r} i_{sq} \tag{3.15}$$

$$\lambda_{rd} = \frac{L_m}{(1 + s\tau_r)} i_{sd}(s) \tag{3.16}$$

The expression for the angel of the dq-axis with respect to the stationary abc-reference frame can then be derived from equation 3.5 and 3.14:

$$\theta_{da}(t) = \int_0^t \omega_d(\tau) d\tau = \int_0^t \frac{L_m}{\tau_r \lambda_{rd}} i_{sq}(\tau) + \omega_r(\tau) d\tau \tag{3.17}$$

The voltage equations can now be simplified to:

$$U_{sd} = \overbrace{R_s i_{sd} + \sigma L_s \frac{d}{dt} i_{sd}}^{U'_{sd}} + \overbrace{\frac{L_m}{L_r} \frac{d}{dt} \lambda_{rd} - \omega_d \sigma L_s i_{sq}}^{U_{sd,comp}} \tag{3.18}$$

$$U_{sq} = \overbrace{R_s i_{sq} + \sigma L_s \frac{d}{dt} i_{sq}}^{U'_{sq}} + \overbrace{\frac{L_m}{L_r} \frac{d}{dt} \lambda_{rd} - \omega_d \sigma L_s i_{sd}}^{U_{sd,comp}} \tag{3.19}$$

Neglecting the last term of the voltage equations the reference value for the voltages can be obtained by current loops with PI controllers as shown in the block diagram in figure 3.10.

The compensation terms of the voltage equations leads to a cross-coupling of the d- and q-axis voltages and if neglected they will act as a disturbance to the system. As discussed in earlier work by the author, see [31], a PI controller can successfully suppress disturbances over a wide frequency range, but if it influence the performance significantly the compensation terms can be calculated analytically and be added to the reference values.

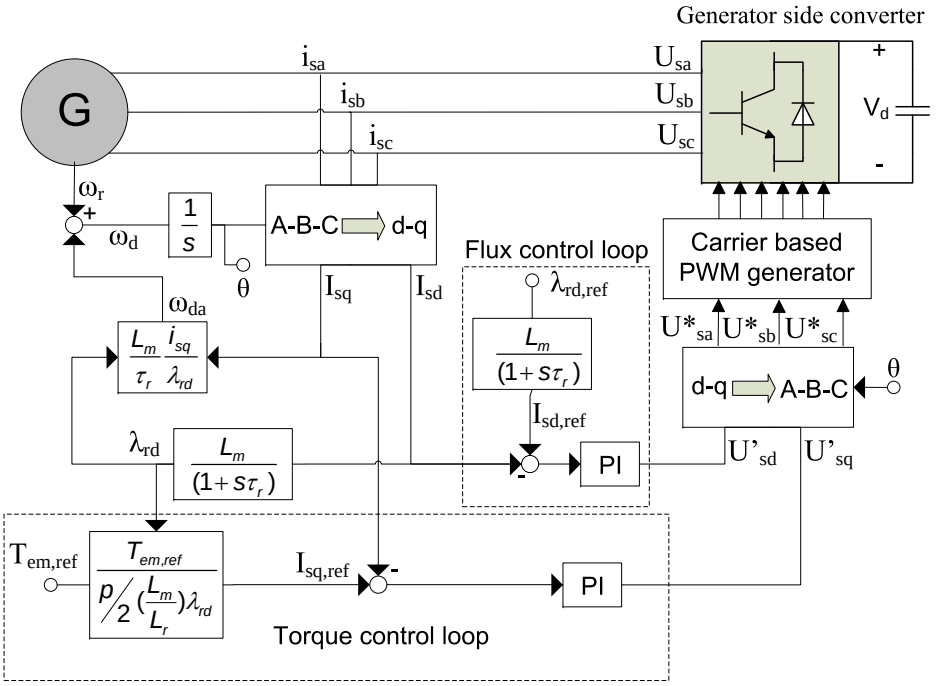

Figure 3.10: Block diagram of field oriented control of an induction generator

3.2.3 Torque and flux control loops

The block diagram of the torque and flux control loop based on the control strategy in figure 3.10 is given in figure 3.11 and 3.12 where the PWM converter is modeled as a first order rational approximation of a time delay T_a equal to half the switching time. No feedback is introduced for the outer torque and flux loops, and the performance of the open loop is dependent of an accurate model between the torque and flux and the currents. Outer feedback loops would increase the complexity of the control system and would require observation of the output values, but should be added if the system does not have the wanted performance.

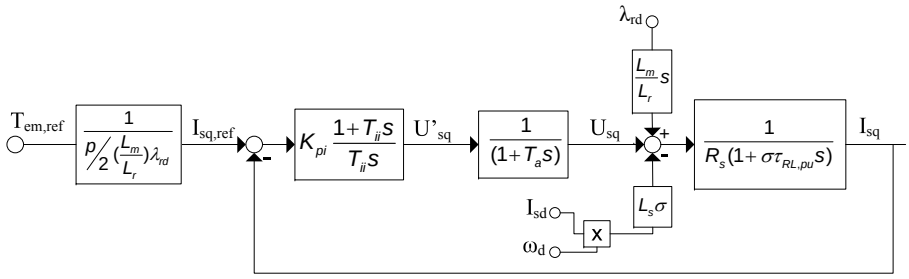

Figure 3.11: Block diagram of the torque control loop

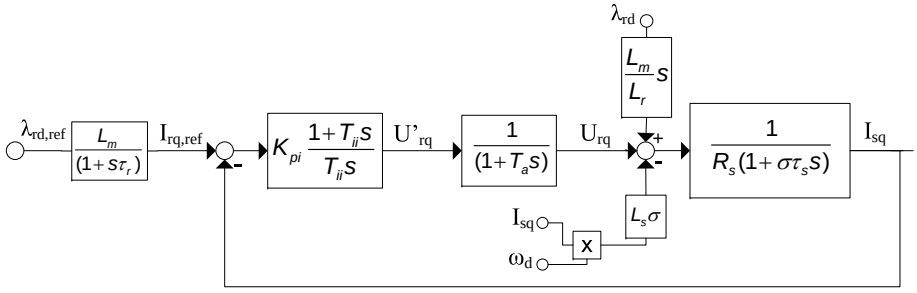

Figure 3.12: Block diagram of the flux control loop

Tuning of the controllers

If a control system has one dominant time constant, and one or several minor time constants, the PI control parameters can be calculated by the Modulus Optimum technique to provide a fast response. The time constant $\sigma\tau_s$ will be the dominating time constant and the MO can be implemented to tune the current controllers. The objective of the method is to cancel the dominant time constant of the system, and to maintain the magnitude of the closed loop transfer function flat and close to unity for as large a bandwidth as possible. The control parameters of the current controllers can then be calculated to 3.20 and 3.21.[?, 32]

$$T_{ii} = \sigma\tau_s \tag{3.20}$$

$$K_{pi} = \frac{\sigma\tau_s R_s}{2T_a} \tag{3.21}$$

3.3 Proposed control strategy

The control strategy of the WEC should improve the power production but at the same time limit the peak to average ratio to respect the rating constraints and energy storage requirements of the system. The work done in [12] shows promising results for control strategies that are based on frequently investigated strategies as passive loading and optimal control, but combined with a power saturation to reduce the power peaks. A mathematical approach to determine control parameters for a single harmonic wave that optimizes the power production while considering a limit on the maximum power is presented.[12] Executed on harmonic waves of different periods and amplitudes a map of advisable control parameters for different waves can be calculated and be used in a look up table to implement wave to wave control if the incident wave's period and amplitude are known. This approach aims to prevent the absorbed power from exceed the power limit given by the saturation level by choosing control parameters that ensure a maximum power production for the incident wave below the limit.

The proposed control strategy in this report is a modified version of the strategy described above where the power saturation level is matched with the rated power of the system and operation above rated speed are enabled. The control parameters can be chose according to passive control or approximate complex-conjugate control and if the absorbed power exceeds the rated power the generator enters the constant power region. Since the reference value for the machinery force may exceed the rated torque of the generator the system will not be able to provide the requested torque in all cases and the proposed control strategy include a saturation of torque. The aim is to utilize the system as much as possible by operating at the power and/or torque saturation level in periods when the incoming wave contains a high energy level. Control parameters that will result in peaks in power and torque above rated values can then be implemented and the power and torque will be saturated so the currents and voltages do not exceed the ratings of the system. With saturation of the power and torque the speed will be the degree of freedom in the system and will limit the operation range. The saturation of the torque will lead to a different response of the WEC than requested by the reference value and the influence of the deviation the must be taken into account when the strategy is evaluated.

Due to the decreased torque capability of the generator in the constant power region this region is more vulnerable for saturation of torque. The speed response of the buoy will be affected by the saturation of torque, and reduced torque capability in combination with big waves (which is the waves that will require over rated speed operation) will lead to an increase in speed compared the unconstrained case. If a sea state can make the generator reach the

pull out speed the production most be shut down, and you get a tradeoff between absorbed power, operation range and torque capability on the one side and rating and costs on the other.

In section 3.2.1 the characteristic of an induction machine that operates with rated torque was analyzed, but the torque of the generator will in this case be given by equation 3.22, where the damping $|\beta_m| = {}^{r_w}/_{n}\,|Z_m|$ is refered to the generator side.

$$T_{em,ref} = |\beta_m|\,\omega_m \tag{3.22}$$

There exists one harmonic wave such that the following relations are fulfilled:

$$T_{em,rated=}\,|\beta_{m,rated}|\,\omega_{m,rated} \tag{3.23}$$

$$P_{m,rated} = T_{em,rated}\omega_{m,rated} = \Re e(3V_{s,rated}I_{s,rated}) \tag{3.24}$$

Figure 3.13 and 3.14 shows the characteristic of the generator in the case of $|\beta_m| < |\beta_{m,rated}|$, $|\beta_m| = |\beta_{m,rated}|$ and $|\beta_m| > |\beta_{m,rated}|$, with the magnetization current kept constant for the first to regions and with the assumption that $\mathbf{V}_s$ is only dependent on the speed.

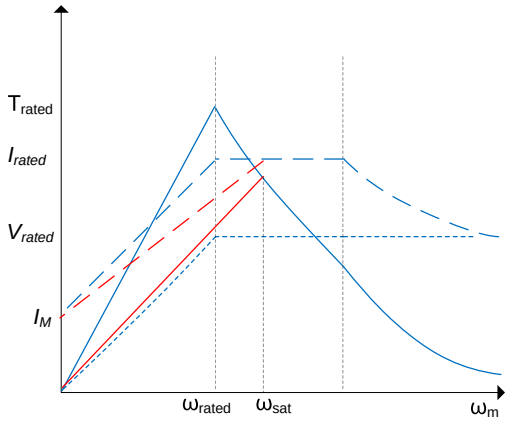

Figure 3.13: Characteristic of the induction generator when$|\beta_m| < |\beta_{m,rated}|$

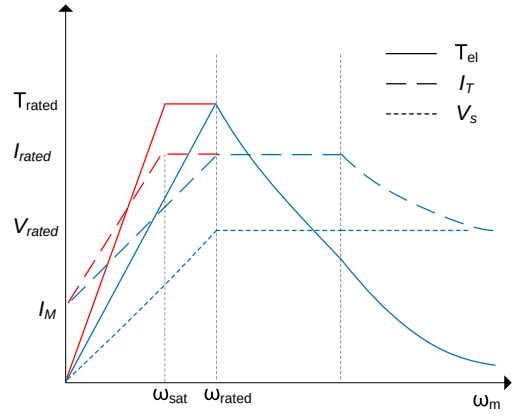

Figure 3.14: Characteristic of the induction generator when $|\beta_m| > |\beta_{m,rated}|$

If the control parameters differ from the rated case the reference torque will not be rated torque at rated speed as seen from equation 3.22 and the figures. In the case of $|\beta_m| < |\beta_{m,rated}|$ the torque is less than rated torque at rated speed and the torque can be increased until the torque capability of the region as shown in figure 3.13. In the case of $|\beta_m| > |\beta_{m,rated}|$ the rated torque will be reached at a speed $\omega_{sat} < \omega_{m,rated}$ and the torque reference must be saturated.

Control of the torque can be realized by use of field oriented control with limitations on the reference values to make sure the currents, voltages and torque does not exceeds its rated values, and the flow chart of the control strategy is shown in figure 3.15.The strategy changes the reference values for the d-axis and q-axis currents directly and the corresponding reference values for the torque and flux are then given by equation 3.15 and 3.16, which are repeated in the figure. The change in the torque reference due to a change in the reference value for the q-axis current is instantaneous while the change in the flux is dependent of the rotor time constant τ_r. The q-axis current can successfully control the torque as long as the dynamics of the current control loop is sufficiently faster than the flux loop.

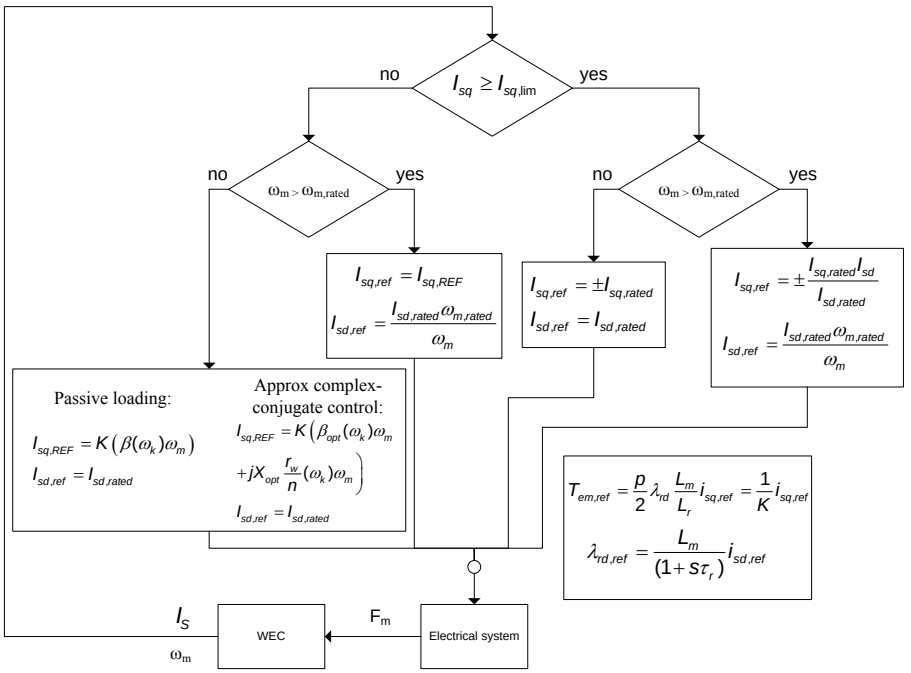

Figure 3.15: Flow chart of the proposed control strategy

Chapter 4

Simulation results

To test the proposed control strategy simulation of a spherical point absorber device with all electric power take of is performed in matlab/simulink based on the mathematical models presented in the two last chapters. The total simulink model is shown in figure 1.1, while the subsystems are given in appendix A. The hydrodynamic parameters, the state space representation of the radiation force and the matlab scripts that calculate the ISSC spectrum and the excitation force is provided by Joergen Hals at the Scentre for Ships and Ocean Structures, while the electrical system is obtained by use of the simulink library SimPowerSystems.

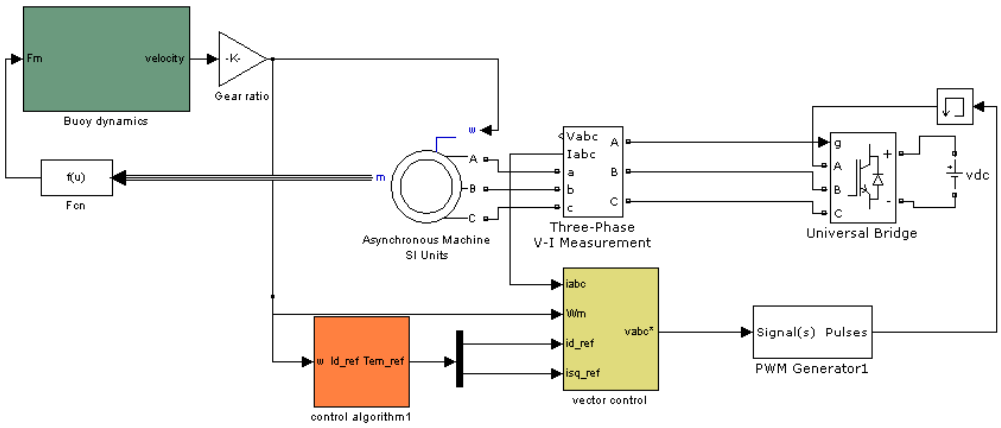

Figure 4.1: Simulink model of the investigated system

The aim of the simulation is to test the practical implementation of the control strategy on a detailed model of the electric system. The first section of the chapter shows time series of the results to validate the control strategy while the last section treats the peak to average ratio for different sea states. To liberate storage the long simulations are performed only with the generator side converter and with a DC-source on the DC-link, which is a valid simplification since the DC-link decouples the electrical system. The parameters for the system are given in table 4.1, where the parameters for the induction generator is obtained from [11], and the DC-link voltage is set to twice the rated voltage of the generator to avoid over modulation. The tuning of the PI controllers are performed according to the Modulus optimum method presented in subsection 3.2.3.

Parameter	Value	Unit	Description
S_n	110	kW	Nominal power generator
V_n	400	V	Nominal voltage generator
ω_{rated}	155.718	$^{rad}/_{s}$	Nominal speed generator
L_m	10.4	mH	Mutual inductance generator
L_s	10.6	mH	Stator inductance generator
L_r	10.6	mH	Rotor inductance generator
R_s	21.6	$m\Omega$	Stator resistance generator
R_r	12.3	$m\Omega$	Rotor resistance generator
p	4	-	Numbers of pole generator
L_l	226	μH	Leak inductance
K_p	0.7835		Gain PI controllers
K_i	21.55		Integral gain PI controllers
U_{dc}	800	V	DC-link voltage
f_{sw}	2000	Hz	Switching frequency
n	20	$-$	Gear ratio
r_w	0.1	m	Pignon radius
J_m	2.3	kgm^2	Mechanical inertia generator
r	5	m	Radius buoy
m	268340	kg	Mass buoy
m_∞		kg	Added mass at infinitely
S	789740	$^{N}/_{m}$	Buoyancy stiffness

Table 4.1: Parameters of the investigated system

The characteristic period is one of the input parameters of the ISSC spectrum and table 2.1 can be used to relate the period to the energy period. The control parameters are chose based on the characteristic period since it corresponds to the reciprocal of the true average frequency. To include the variance of the parameters of the real ocean wave and to provide

average measures of the sea state the simulation period of the system has to be long enough, but at the same time sufficiently short so that the wave conditions can be assumed stationary. A simulation time of 90 seconds is used for simulations for irregular waves. From the values given in table 4.1 and equation 3.15 the rated value for the torque and the rated q-axis current are found to be 327.16 Nm and 268.375 A[1].

The simulation model is based on the following simplifications:

- No friction
- No satuaration of currents and voltages in the generator
- No core losses
- The point absorber only move in heave
- Linear wave theory
- Plane waves

[1]The rated active power of the generator is low compared to the rated apparent power due to a bad power factor. This problem should be addressed, but is out of the scope of the work done in this report.

4.1 The performance of the proposed control strategy

To investigate the performance of the algorithm presented in 4.2 simulations with irregular waves with a significant wave height of 1.41 meters and energy period of 6 seconds are performed. The produced power given in figure 4.3 is measured at the DC-link and are filtered by a first order low pass filter with cut off frequency of $100\,^{rad}/_{s}$. The control parameters are chosen according to the optimal damping in the case of passive loading and the excitation force, the speed and the position of the buoy are given in figure 4.2 for a time series of 90 seconds. For the applied characteristic period the optimal damping R_m is $100.74\,^{kg}/_{s}$ and the corresponding speed $\omega_{m,sat}$ where the q-axis current will attain its rated value is then $0.65\,^{m}/_{s}$. Consequentley will the system reach both torque and power saturation during the time series.

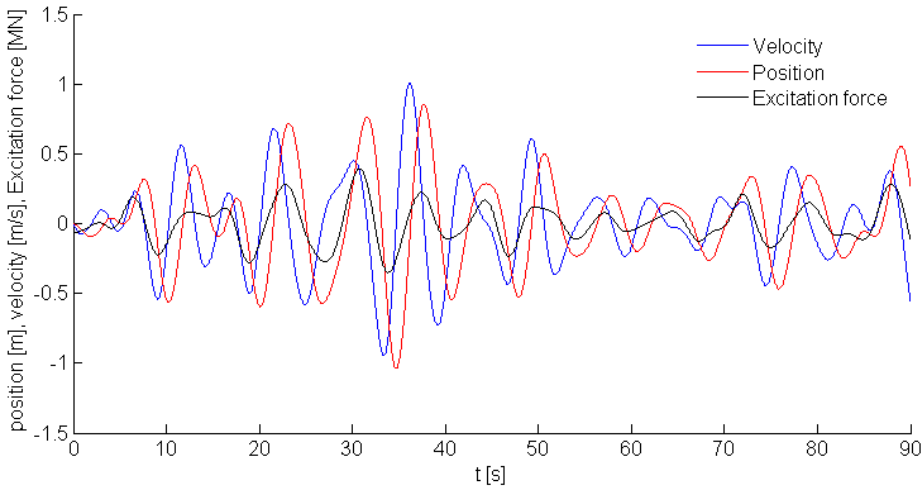

Figure 4.2: Excitation force, velocity, and position for irregular waves ($H_{1/3}$ = 1.41m , T_1 = 5.41s)

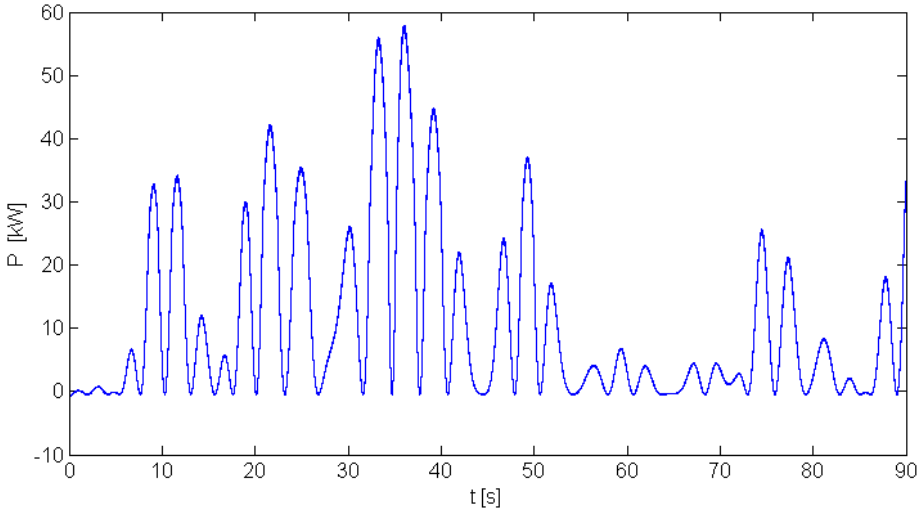

Figure 4.3: Filtered power for irregular waves ($H_{1/3} = 1.41$m , $T_1 = 5.41$s)

Figure 4.4 shows the reference values and the measured values of the torque and q-axis current for a section of the time series where the system reach both its power and torque limits and a fast and accurate control are obtained. Between 32 and 38 seconds the generator enters the constant power region and the reference value for the d-axis current drops in inverse ratio with the speed as shown in figure 4.5. As a consequence the torque capability of the generator drops with the same ratio as the change in flux due to the reduced d-axis current and the speed of change in flux and torque is limited by the rotor time constant. The time delay in the flux weakening leads to a small overvoltage compared to the rated value since the flux is not decreased sufficiently fast enough to compensate for the voltage increase due to the over rated speed. If the system cannot handle the voltage for the applied time the speed limitation can be decreased to respect the dynamic of the rotor flux. Alternatively a feedback loop could be introduced in the flux control loop to make the reference value of the d-axis current drop faster to obtain a faster decrease in flux, but a limit on the reference value must then be applied to avoid high reference values when the flux should be increased again. The over voltage also result in a peak power somewhat higher than the rated power for about a second as shown in figure 4.3.

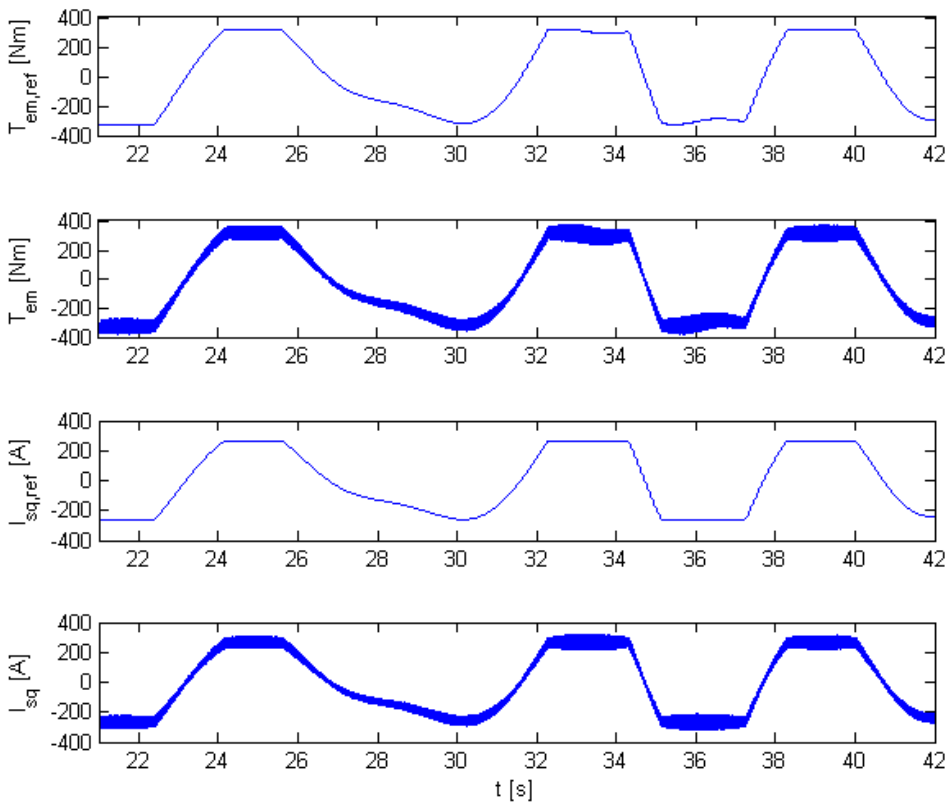

Figure 4.4: Torque and q-axis reference values and instantenous values during power and torque saturation for irregular waves ($H_{1/3} = 1.41$m , $T_1 = 5.41$s)

Figure 4.6 shows the filtered applied three phase voltages at the generator terminals, the speed of the generator and the three phase currents. The amplitude of the currents are saturated when the speed exeeds $129.9\,^{rad}/_{s}$(corresponding to $0.65\,^{m}/_{s}$) and the deformation of the voltage amplitude due to the flux weakening can be observed.

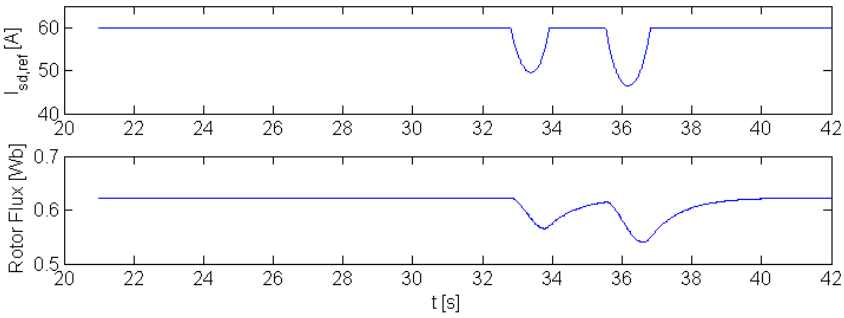

Figure 4.5: Reference value for the d-axis stator current and the estimated flux for for irregular waves ($H_{1/3} = 1.41\text{m}$, $T_1 = 5.41\text{s}$)

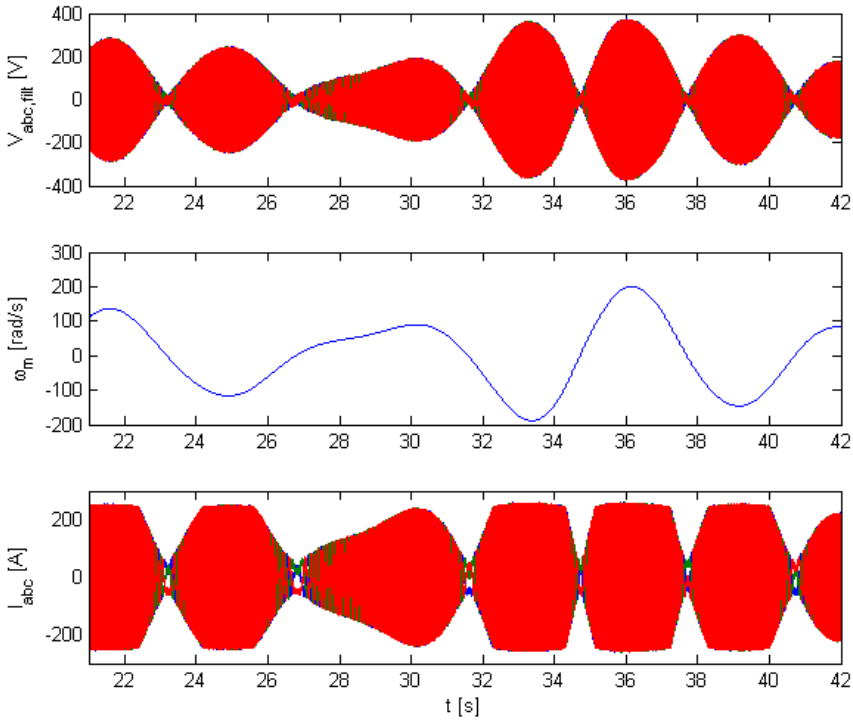

Figure 4.6: Filtered three phase stator voltages, speed and three phase stator currents for irregular waves ($H_{1/3} = 1.41\text{m}$, $T_1 = 5.41\text{s}$)

4.2 The peak to average ratio for passive loading and irregular waves

In section 2.2.2 an electric analogue was obtained where the hydrodynamic and mechanical parameters was represented by a impedance $Z_b(\omega)$ and the variance of the different terms with regard to the frequency is given in figure 4.7.

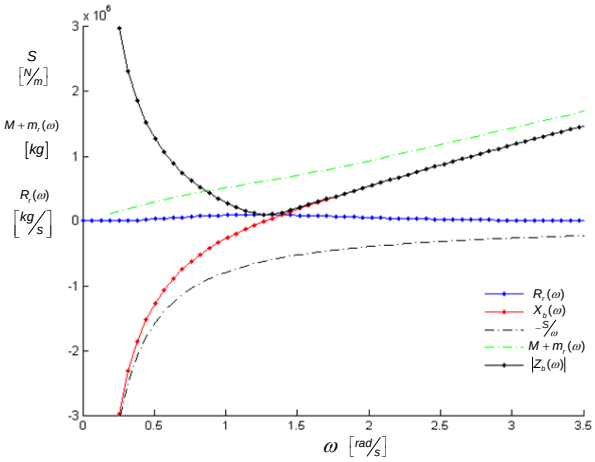

Figure 4.7: The hydrodynamic paramters as a function of the frequency for the point absorber in heave

The total mass of the system was given by $M = m + J_{eq}g_r^2$ and the gear ratio $g_r = {}^{n}/_{r_w}$ contributes to canceling the capacitive term caused by the buoyancy stiffness This effect is useful if it changes the natural frequency of the device in the direction of the periods of the waves for the sea states the device is designed for. The black dotted line in figure 4.7 shows the amplitude of the buoy impedance, which correpspond to the amplitude of the optimal damping for both passive and complex conjugate control according to section 2.3 and with the chosen gear ratio the natural frequency of the buoy is reduced to a value between 1 and 1.5 ${}^{rad}/_{s}$. The required torque by the control strategies will then be reduced for waves in that frequency range since the damping is reduced compared to the case without the gear, an additional effect to the reduced torque requirements that a gear introduces. This also affect the peak to average ratio in a positive way since the required reactive power by the

mechanical and hydrodynamic system is reduced, which reduces the peak power the electric system must provide. So for WEC that have a small natural frequency compared to the waves a gear represents an extra benefit in addition to the increased speed and the reduced torque requirements as the peak to average ratio also will decrease.

Table 4.2 shows an example for a scatter diagram with values from Westhinder on the Belgian continental shelf and the diagram provides statistic data of average occurrence in percent for different sea states for one year.[33] The information can be used to design and rate a device for a specific location. The values in table 4.2 are typical for the north sea[33] and the characteristic sea state for this area typically consist of small waves. Based on the values in the table three different sea states are picked out to test the performance of the system for different relevant operation conditions, $H_{1/3} = 2.8m/T_1 = 6.53s$, $H_{1/3} = 1.41m/T_1 = 5.41s$ and $H_{1/3} = 1.3/T_1 = 3.83s$. Passive loading with $R_m = R_{m,opt}(\omega_1)$ are implemented, and simulations are performed for each sea state with the proposed control algorithm and also without any special actions to prevent the system to exceed its ratings. Figure 4.8 shows the machinery damping for the three test cases, and the wave with the smallest period require the largest damping as seen from the figure. The value $R_{m,rated} = ({}^{n}/_{r_w})^2 \beta_{rated}$ which correspond to the damping that would give rated torque at rated speed is lower than the minimum value for $R_{m,opt}$ and torque will consequently reach its rated value before rated speed for all sea states.

$T_1\ [s]$ / $H_{1/3}\ [m]$	≤ 2.5	2.5– 3.5	3.5– 4.5	4.5– 5.5	5.5– 6.5	6.5– 7.5	7.5– 8.5	≥ 8.5 –3.5	Sum
≤ 0.25		0.06	0.64	0.21	0.02				0.93
$0.25 - 0.5$	0.05	4.46	11.69	3.86	0.53	0.06	0.01		20.65
$0.5 - 1$	0.01	6.12	20.51	8.38	1.91	0.30	0.02		37.25
$1 - 1.5$	-	0.29	10.63	8.98	1.83	0.27	0.02	0.00	22.02
$1.5 - 2$		-	1.89	6.46	2.02	0.27	0.01	0.00	10.65
$2 - 2.5$			0.04	2.67	2.00	0.42	0.01	0.00	5.14
$2.5 - 3$			-	0.57	1.17	0.50	0.02	0.00	2.27
$3 - 3.5$				0.04	0.46	0.26	0.04	-	0.79
$3.5 - 4$				-	0.09	0.07	0.05		0.21
$4 - 5.5$					0.02	0.03	0.02		0.07
$5.5 - 6$					-	0.01	-		0.02
≥ 6						-			-
	0.06	10.93	45.4	31.17	10.04	2.20	0.20	0.01	100

Table 4.2: Typical scatter diagram for all wave directions for Westhinder (Belgian contonental shelf)

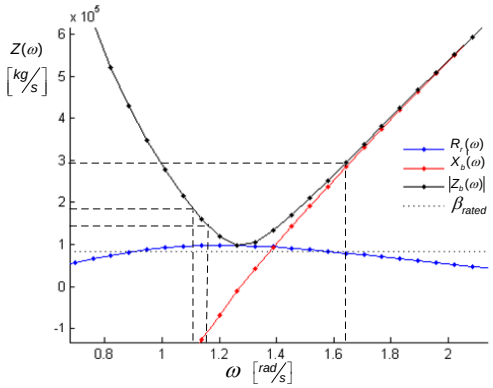

Figure 4.8: The hydrodynamic parameters as a function of the frequency for the point absorber in heave. The dotted lines marks the amplitude of the optimal damping for both passive and complex conjugate control for harmonics waves of period $5.63\,s$, $5.41\,s$ and $3.84\,s$.

The results for the simulations are summarized in table 4.3, where the subscript c denote the results for the constrained cases, and plot of the results are given in appendix B. For $H_{1/3} = 1.41m/T_1 = 5.41s$ and $H_{1/3} = 1.3/T_1 = 3.83s$ the implemented control strategy successfully manage to keep the system from exceeding its rated values (a small deviation from the rated peak power occur for $H_{1/3} = 1.41m/T_1 = 5.41s$ as discussed in the last section) and the peak to average ratio k is reduced compared to the unconstrained case. For the smallest wave the mean power production actually increase compared to the unconstrained case and since this sea state resulted in the largest deviation in the WECs natural frequency compared to the waves as shown in figure 4.8 this can be caused by introduction of a complex term in the torque when the torque is saturated. Also the sea state $H_{1/3} = 1.41m/T_1 = 5.41s$ obtain good results and only a small reduction in average produced power is introduced. At the same time the peak torque is reduced from $620\,Nm$ to its rated value and the peak to average ratio is reduced to 5.51. As discussed in chapter 2 the maximum speed increase for the proposed strategy and the system is more exposed for reaching the pull out speed. Since the machinery resistance is less than the rated value the peak power will be given by $\hat{P} = T_{em,rated}\omega_{m,max}$ and for the sea state with the smallest produced power the speed never reach its rated level and the peak power is consequently less than rated power.

	$T_1 = 3.83\,s$	$T_1 = 5.41\,s$	$T_1 = 6.53\,s$
	$H_{1/3} = 1.3\,m$	$H_{1/3} = 1.41\,m$	$H_{1/3} = 2.8\,m$
$R_{m,opt}\,[k\frac{kg}{s}]$	294.63	142.38	176.82
$\overline{P}\,[kW]$	5.35	11.483	51.37
$\overline{P}_c\,[kW]$	5.78	10.317	25.94
$\hat{P}[kW]$	37.11	99.97	453.30
$\hat{P}_c\,[kW]$	26.62	56.86	86.14
$\hat{\omega}_m\,[rad/s]$	70.4	165.5	328.4
$\hat{\omega}_{m,c}\,[rad/s]$	85.1	200.8	463.5
k/k_r	6.94/9.52	8.7/-	8.82/–
$k_c/k_{c,r}$	4.61/8.81	5.51/-	3.32/1.96

Table 4.3: System repsons with and without the proposed control strategy for three differents sea states

For the $H_{1/3} = 2.8m/T_1 = 6.53s$ the system does not manage to keep the rating of the system. The maximum speed is $463.4\,{}^{rad}/_{s}$ and for a conventional generator the pull out speed is reached. Weakening the flux is not efficient to keep the voltage down any more since the voltage drop across the $j\omega_e {}^{L_m^2}/_{L_r}$ is no longer the dominant one. If the system is going to operate during this sea condition the rating of the system must be increased.

Chapter 5

Conclusion

Introductorily the aim of this thesis was concretized to be development and implementation of a reliable control strategy of a WEC that respect the ratings and energy storage requirements of the electrical system while improving the absorbed power under the given constrains. The proposed control strategy saturates the torque and power when it exceeds its rated values by controlling the flux and torque indirectly by implementing current regulators on the q-axis and d-axis currents and to utilize the electrical system better operation above rated speed was tolerated. The strategy was validated by the performed simulations and for two of the sea states the average produced power was barley affected while the peak to average ratio was reduced considerably. A low peak to average ratio will give a more cost efficient device since the rating of the electrical system can be decreased and the energy storage requirements are reduced. As the torque and power is saturated the speed will be the degree of freedom of the system and the proposed strategy will result in a higher maximum speed compared to the unconstrained case. The limitation of the strategy will then be the pullout speed of the generator.

The results shows that the power production is dependent on the sea state, the chosen control parameters and the saturation level of power and torque and based on measured date the rating of the system should be the optimized according to the distribution of energy on the different sea states for the specific locations. When the rating of the system is determined the proposed control strategy can be implemented and the control parameters can be optimized on a sea state to sea state or a wave to wave basis to utilize the system as good as possible under the limitations of the system given by the ratings and the pulout speed.

The investigated system had a two step linear to rotational gear which introduces not only

a lower torque requirement for the generator and a higher speed, but also a change in the natural frequency of the device. For the system the change moved the natural frequency of the device closer to the frequency range of the incoming waves and the required torque/machinery force from passive loading or complex conjugate control is then reduced. Additionally will the peak to average ratio decrease since the system do not have to provide the mechanical and hydrodynamic system with the same amount of reactive power and compensating the natural frequency of the system mechanically improves the design specifications for the electrical system considerably. The slow and irregular nature of the ocean waves gives different requirements to the generator than to the conventional generators used in power production and the generator should be design to have a high torque capability, low speed and a high pullout speed.

5.1 The contribution of the work

The main contribution to the field of research by the work done in this thesis is by the author recognized to be:

- Development of a control algorithm that enable non linear control of a WEC to respect the ratings of the electric power take off and limit the peak to average ratio while maximizing the power production.
- Identification of the limitations of the electrical Power Take Off and evaluations of the consequences

5.2 Further work

Based on the results in this work further research should be addressed to the following topics:

- The proposed control strategy should be tested for different saturation levels, control parameters and sea states
- A Model Predictive Control algorithm that optimizes the saturation level based on the wave climate of the chosen location and the control parameters with respect to the ratings and pull out speed.
- Further research on generator design for Wave Energy Converters

- Building a more accurate model that includes the copper losses. Flux weakening below rated speed should then be investigated to improve the efficiency of the generator for small loads

Bibliography

[1] Carbontrust. Ocean waves and wave energy design.

[2] N. Mohan, T. Undeland, and W. Robbins. *Power Electronics- Converters, Application and Design*. John Wiley and Sons, Inc, 2003.

[3] AEA Energy and Environment. *Review and analysis of ocean energy systems development and supporting policies*. Implementing agreement on ocean energy systems, 2006.

[4] G. Hagerman. Southern New England Wave Energy Resource Potential. *EPRI, March*, 2001.

[5] D. Mollison S. Barstow, G. Moerk and J. Cruz. The wave energy resource. In *Ocean wave energy: current status and future prepectives*. Springer, 2008.

[6] J. Falnes. A review of wave-energy extraction. *Marine Structures, vol.20 no.4*, 20(4):185–201, 2007.

[7] G Bhuyan J. Khan. Ocean energy: Global technology development status. Technical Report T0104, Powertech Labs for the IEA-OES, 2009.

[8] J Hals. *Modelling and phase control of wave-energy converters*. PhD thesis, NTNU.

[9] J. Falnes. Principles for capture of energy from ocean waves. phase control and optimum oscillation. Technical report, Department of Physics, NTNU, 1997.

[10] H. Polinder and M. Scuotto. Wave energy converters and their impact on power systems. In *Future Power Systems, 2005 International Conference on*, pages 1–9, 2005.

[11] E. Tedeschi, M. Molinas, M. Carraro, and P. Mattavelli. Analysis of Power Extraction from Irregular Waves by All-Electric Power Take Off.

[12] E. Tedeschi and M. Molinas. Control strategy of wave energy converters optimized under power electronics rating constrains. *3rd international conference on Ocean Energy (ICOE10)*, pages 1 –6, oct 2010.

[13] E. Tedeschi and M. Molinas. Impact of control strategies on the rating of electric power take off for wave energy conversion. *ISIE2010, Bari*, 2010.

[14] Johannes Falnes. A review of wave-energy extraction. *Marine Structures*, 20(4):185 – 201, 2007.

[15] L.H. Holthuijsen. *Waves in oceanic and coastal waters*. Cambridge Univ Pr, 2007.

[16] J. Falnes. *Ocean waves and oscillating systems: linear interactions including wave-energy extraction*. Cambridge Univ Pr, 2002.

[17] Turgut "Sarp" Sarpkaya. *Wave Forces on Offshore Structures*. Cambridge Univ Pr, 2010.

[18] W.H. Michel. Sea spectra simplified. *Marine Technology*, 5(1):17–30, 1968.

[19] W.H. Michel. Sea spectra revisited. *MAR TECHNOL*, 36(4):211–227, 1999.

[20] Reza Taghipour, Tristan Perez, and Torgeir Moan. Hybrid frequency-time domain models for dynamic response analysis of marine structures. *Ocean Engineering*, 35(7):685 – 705, 2008.

[21] J. Falnes. Principles for capture of energy from ocean waves: phase control and optimum oscillation. *Internet Web page. h http://www. phys. ntnu. no/instdef/prosjekter/bolgeenergi/phcontrl. pdf i*, 1997.

[22] H. Polinder, MA Mueller, M. Scuotto, and M.G. de Sousa Prado. Linear generator systems for wave energy conversion. In *Proceedings of the 7th European Wave and Tidal Energy Conference, Porto, Portugal*, 2007.

[23] M. Molinas, O. Skjervheim, P. Andreasen, T. Undeland, J. Hals, T. Moan, and B. Sorby. Power electronics as grid interface for actively controlled wave energy converters. In *Clean Electrical Power, 2007. ICCEP '07. International Conference on*, pages 188 –195, 2007.

[24] K. Burges D. Broad. Technical and operational barriers to integration of wave energy. Technical report, Oregon Wave Energy Trust -Utility Market Initiative, 2009.

[25] G. Daltion D. O'Sullivan. Challanges in the grid connection of wave energy devices. In *Proceedings of the 8th European Wave and Tidal Energy Conference,Uppsala, Sweden, 2009*, pages 12 –20, 2009.

[26] E.P. Wiechmann, P. Aqueveque, R. Burgos, and J. Rodriguez. On the efficiency of voltage source and current source inverters for high-power drives. *Industrial Electronics, IEEE Transactions on*, 55(4):1771 –1782, 2008.

[27] W. Deprez, A. Dexters, J. Driesen, and R. Belmans. Energy efficiency of small induction machines: comparison between motor and generator mode. *ICEM 2006*, pages 2–5, 2006.

[28] A. Testa, S. De Caro, and T. Scimone. High efficiency field oriented control of an induction generator for a tidal current turbine. In *Power Electronics and Applications, 2009. EPE '09. 13th European Conference on*, pages 1 –10, 2009.

[29] N. Mohan. *Advanced electric drives*. MNPERE, 2001.

[30] X. Xu and D.W. Novotny. Selection of the flux reference for induction machine drives in the field weakening region. *Industry Applications, IEEE Transactions on*, 28(6):1353 –1358, 1992.

[31] E. Bjoernstad. Control of gride side converter for grid connection of wave energy converters. Master's thesis, NTNU, 2010.

[32] J.A. Suul, M. Molinas, L. Norum, and T. Undeland. Tuning of control loops for grid connected voltage source converters. In *Power and Energy Conference, 2008. PECon 2008. IEEE 2nd International*, pages 797 –802, 1-3 2008.

[33] C. Beels, JCC Henriques, J. De Rouck, MT Pontes, G. De Backer, and H. Verhaeghe. Wave energy resource in the North Sea. 2007.

[34] J. Svensson O.Carlson, A.Grauers and AA. Larsson. A comparision between electrical systems for variable speed operation of wind turbines. In *European Wind Energy Association Conference and Exhibition (EWEC'94)*, pages 500 –505, October 1004.

Appendix A

Simulation model

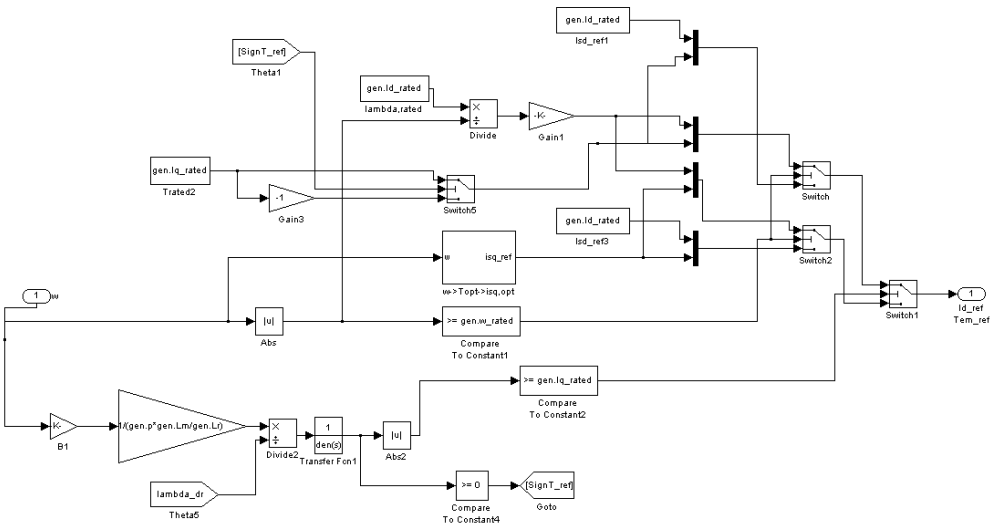

Figure A.1: Subsystem Control algorithm

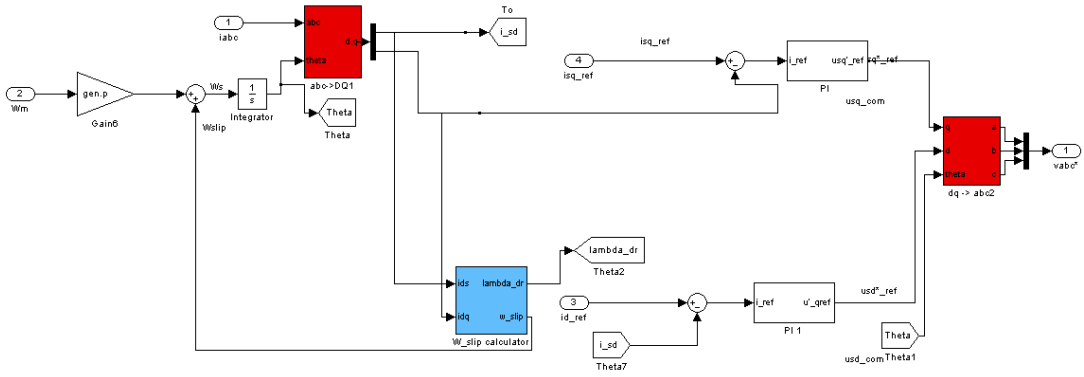

Figure A.2: Subsystem vector control

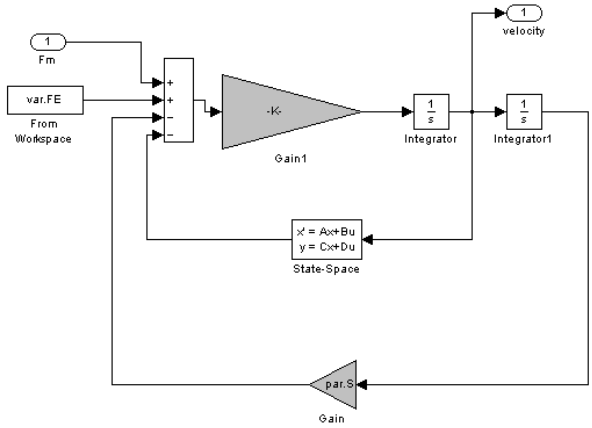

Figure A.3: Subsystem Buoy dynamic

Appendix B

Results

B.1 Results for $T_1 = 3.83\,s$ and $H_{1/3} = 1.3\,m$

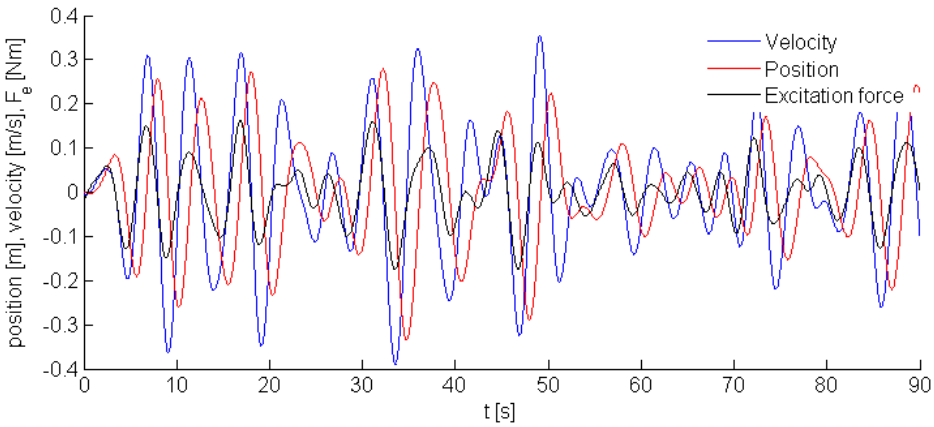

Figure B.1: Excitation force, velocity, and position for the unconstrained case for irregular waves ($H_{1/3} = 1.3$m , $T_1 = 3.83$s)

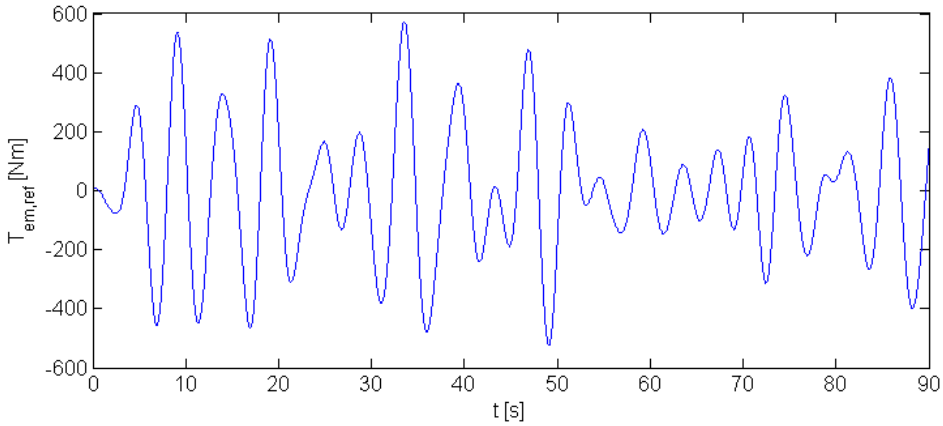

Figure B.2: The torque reference value for the uncontrained case for irregular waves ($H_{1/3} = 1.3$m , $T_1 = 3.83$s)

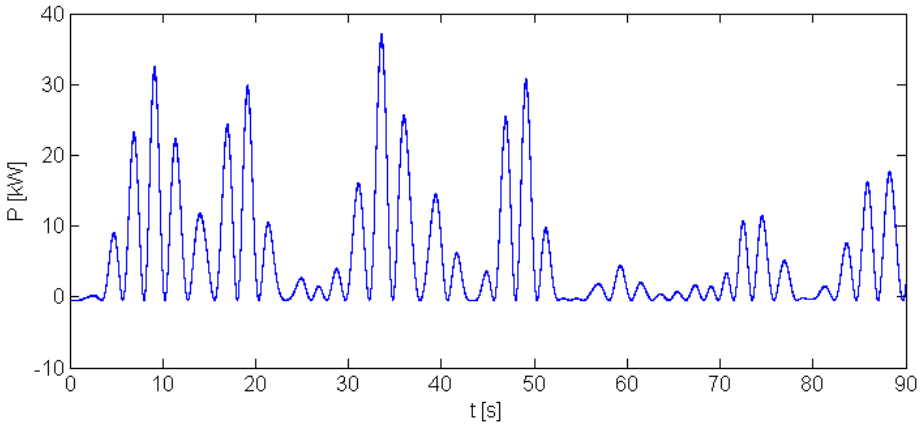

Figure B.3: Produced power for the unconstrained case for irregular waves ($H_{1/3} = 1.3$m , $T_1 = 3.83$s)

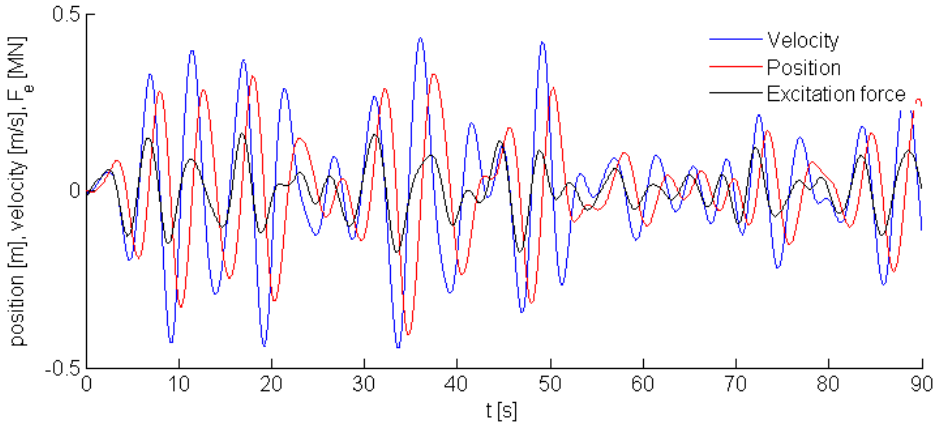

Figure B.4: Excitation force, velocity, and position for the constrained case for irregular waves ($H_{1/3} = 1.3$m , $T_1 = 3.83$s)

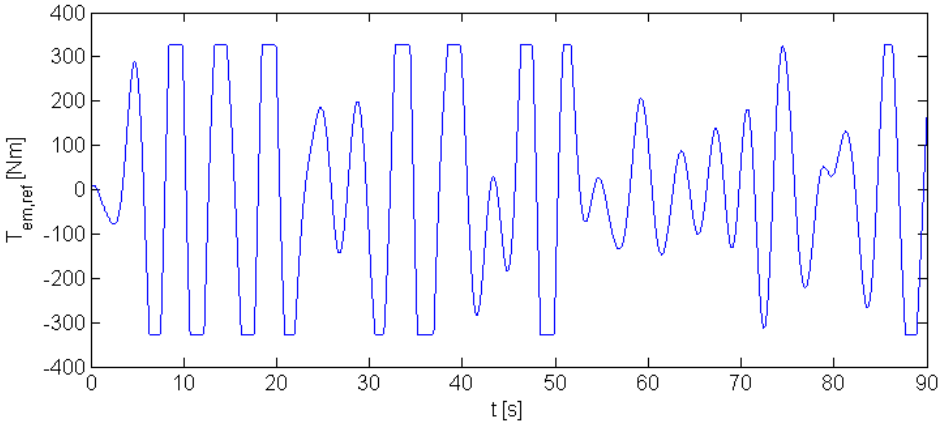

Figure B.5: The torque reference value for the contrained case for irregular waves ($H_{1/3} = 1.3$m , $T_1 = 3.83$s)

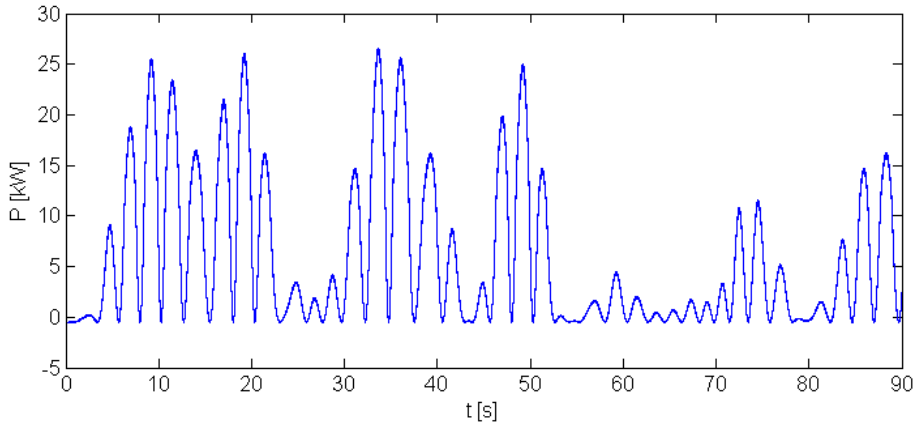

Figure B.6: Produced power for the constrained case for irregular waves ($H_{1/3}$ = 1.3m , $T_1 = 3.83$s)

B.2 Results for $T_1 = 5.41\,s$ and $H_{1/3} = 1.41\,m$

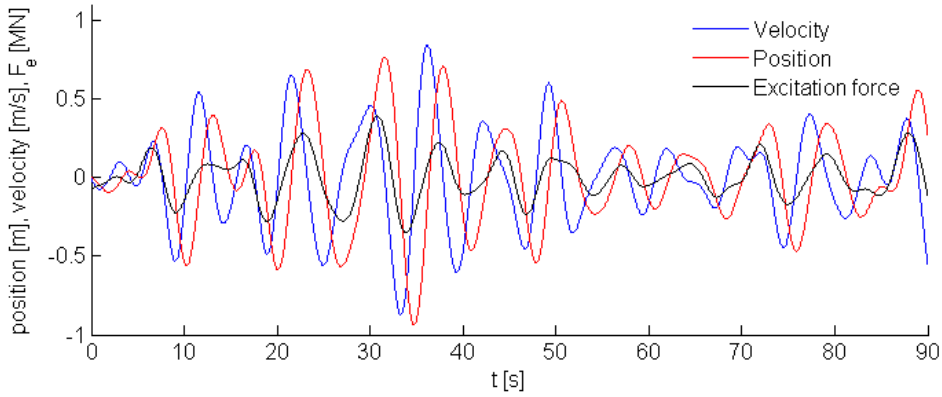

Figure B.7: Excitation force, velocity, and position for the unconstrained case for irregular waves ($H_{1/3} = 1.41$m , $T_1 = 5.41$s)

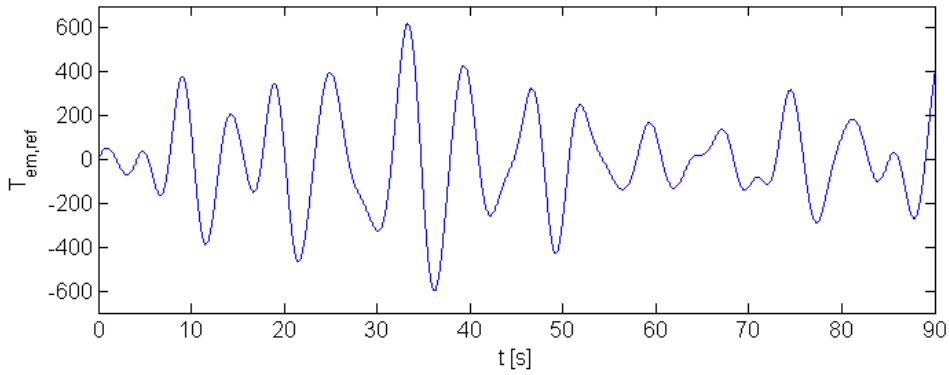

Figure B.8: The torque reference value for the uncontrained case for irregular waves ($H_{1/3} = 1.41$m , $T_1 = 5.41$s)

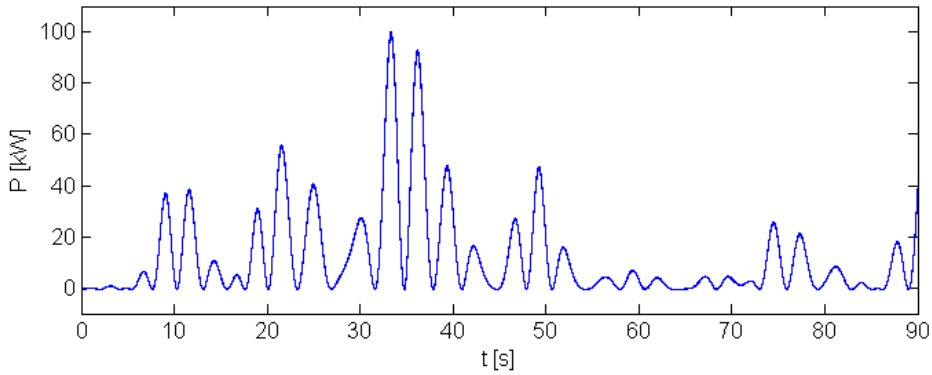

Figure B.9: Produced power for the unconstrained case for irregular waves ($H_{1/3} = 1.41$m , $T_1 = 5.41$s)

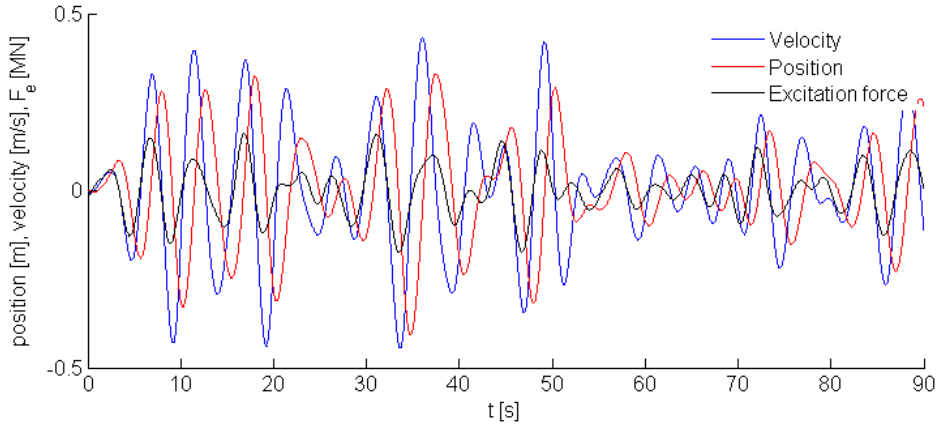

Figure B.10: Excitation force, velocity, and position for the constrained case for irregular waves ($H_{1/3} = 1.41$m , $T_1 = 5.41$s)

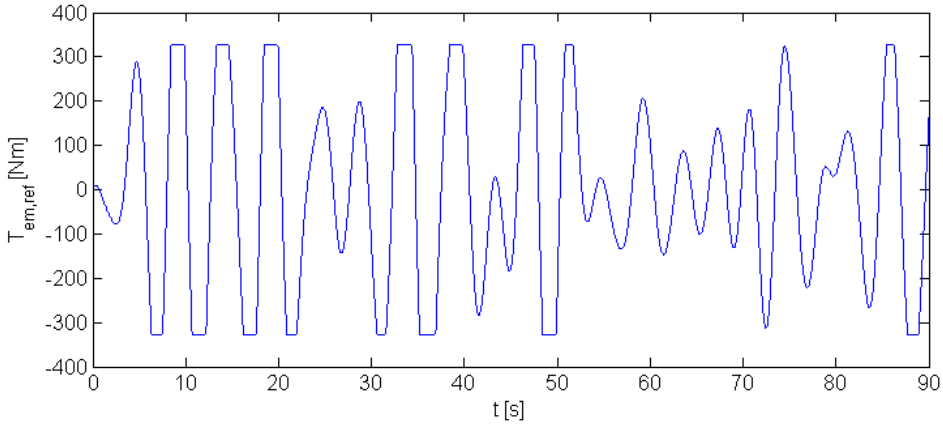

Figure B.11: The torque reference value for the contrained case for irregular waves ($H_{1/3} = 1.41$m , $T_1 = 5.41$s)

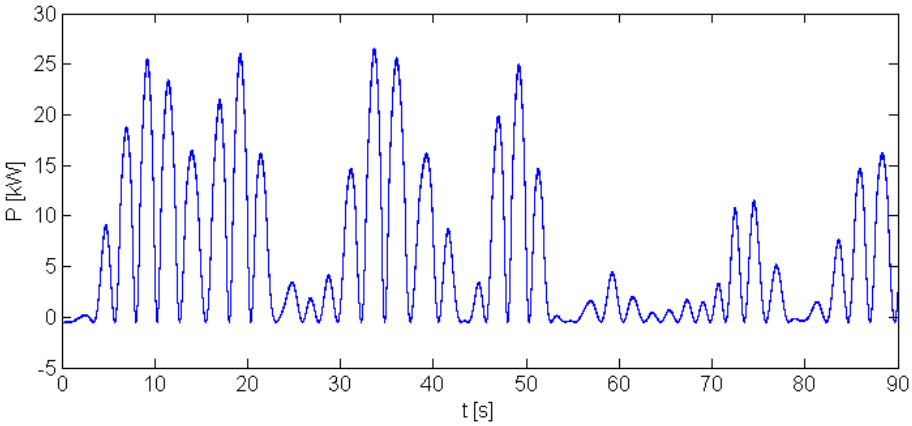

Figure B.12: Produced power for the constrained case for irregular waves ($H_{1/3} = 1.41$m , $T_1 = 5.41$s)

B.3 Results for $T_1 = 6.53\,s$ and $H_{1/3} = 2.8\,m$

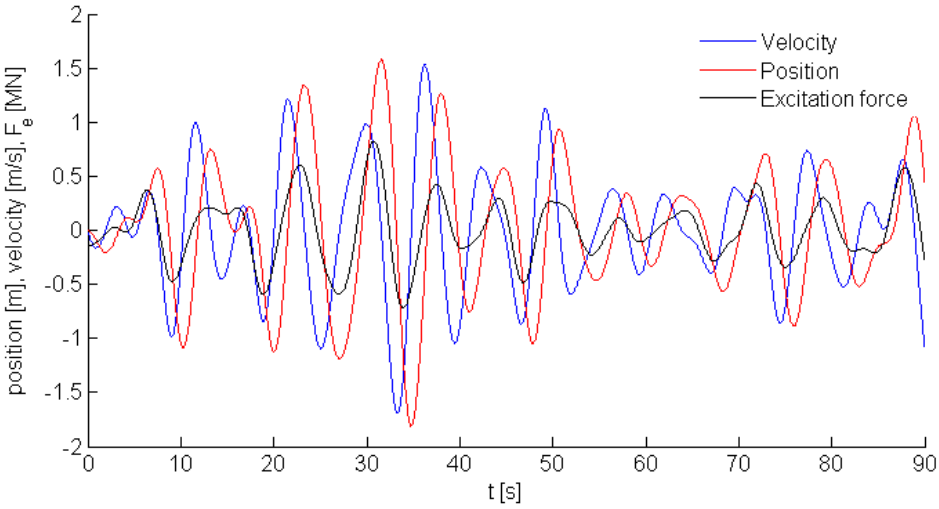

Figure B.13: Excitation force, velocity, and position for the unconstrained case for irregular waves ($H_{1/3} = 2.8$m , $T_1 = 6.53$s))

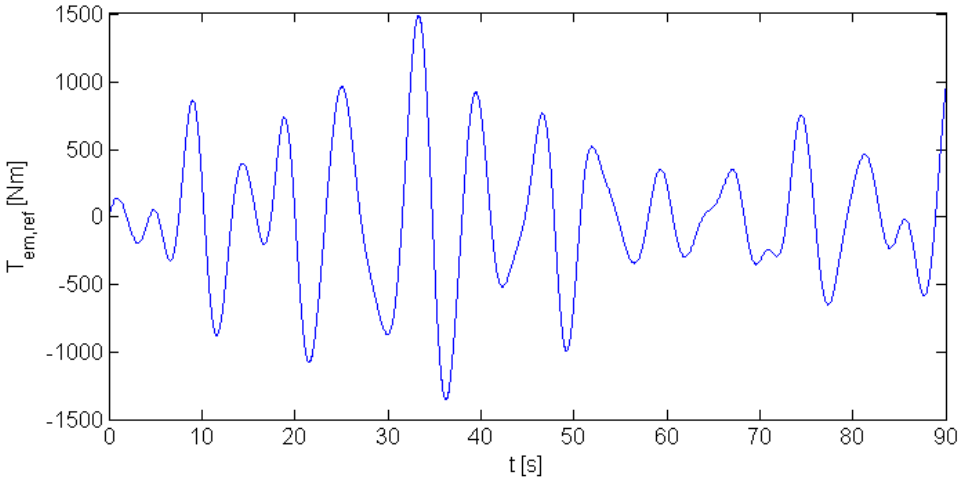

Figure B.14: The torque reference value for the uncontrained case for irregular waves ($H_{1/3} = 2.8$m , $T_1 = 6.53$s)

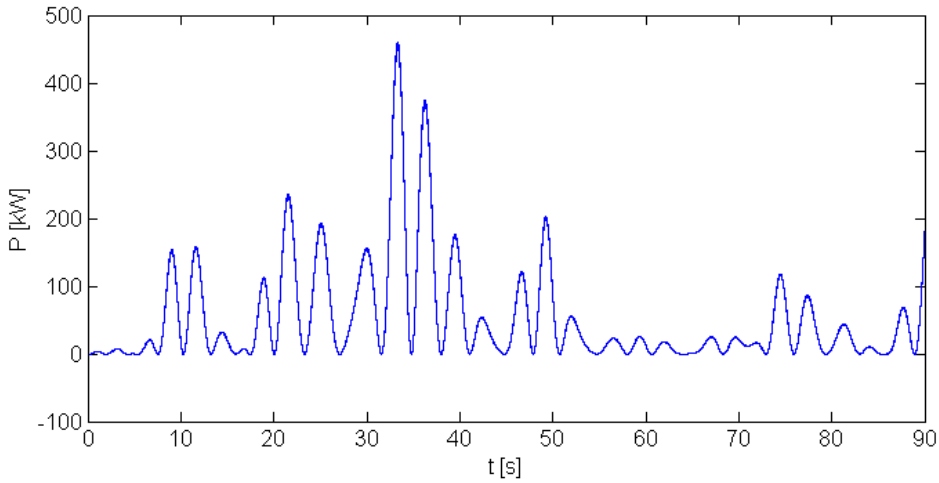

Figure B.15: Produced power for the unconstrained case for irregular waves ($H_{1/3} = 2.8$m , $T_1 = 6.53$s)

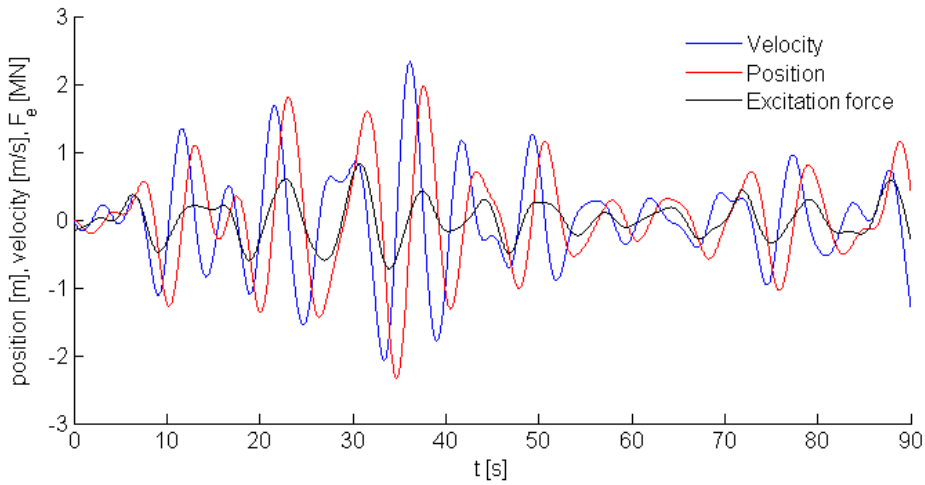

Figure B.16: Excitation force, velocity, and position for the constrained case for irregular waves ($H_{1/3} = 2.8$m , $T_1 = 6.53$s)

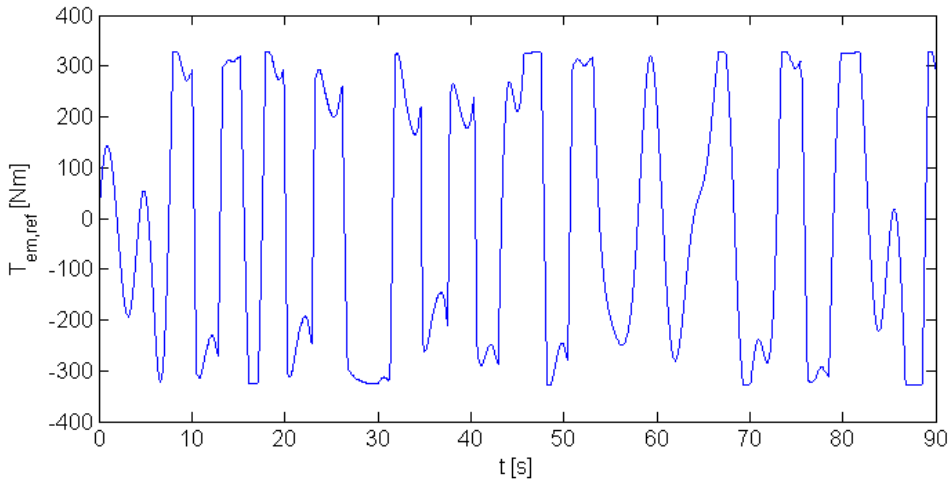

Figure B.17: The torque reference value for the contrained case for irregular waves ($H_{1/3} = 2.8$m , $T_1 = 6.53$s)

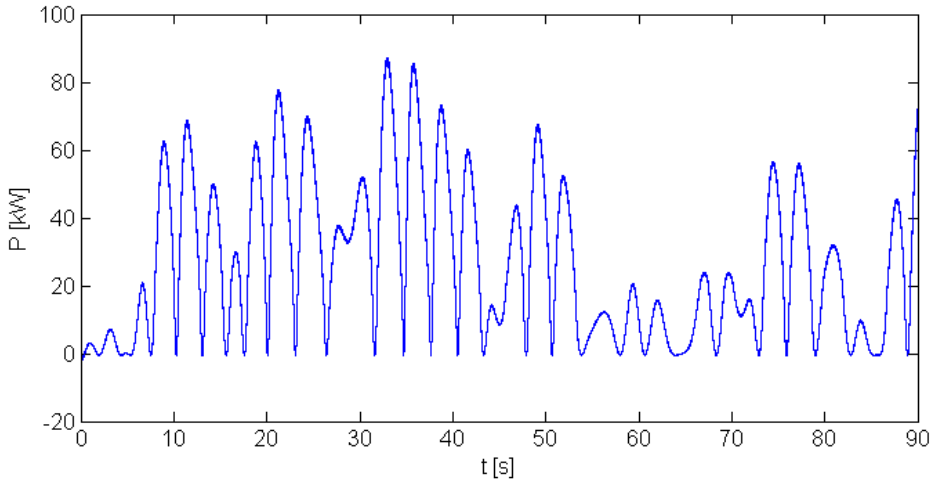

Figure B.18: Produced power for the constrained case for irregular waves ($H_{1/3} = 2.8$m , $T_1 = 6.53$s)

Appendix C

Voltage source converter

A forced commutated converter as the VSC can provide sinusoidal currents by use of switching schemes techniques like Pulse-Width-Modulation (PWM), and the only harmonics present will be of high order around the switching frequency [34].Insulated Gate Bipolar Transistor (IGBT) can provide switching frequencies up to about 5 to 10 kHz, and the evolution of the devices with a view of increase the power rating and reduce the costs are fast [34]. Therefore a VSC with IGBTs can provide both sufficient switching frequencies to maintain an acceptable level of harmonics and a high power rating.

Figure C.1: Three-leg voltage source converter

C.1 Modulation

There exist several modulation methods for VSC, both voltage and current regulated. The control strategy presented in chapter 3 requires a voltage regulated modulation type, and a carrier based PWM is used due to its simple implementation. Figure C.2 shows the basic consept of a carrier based PWM.

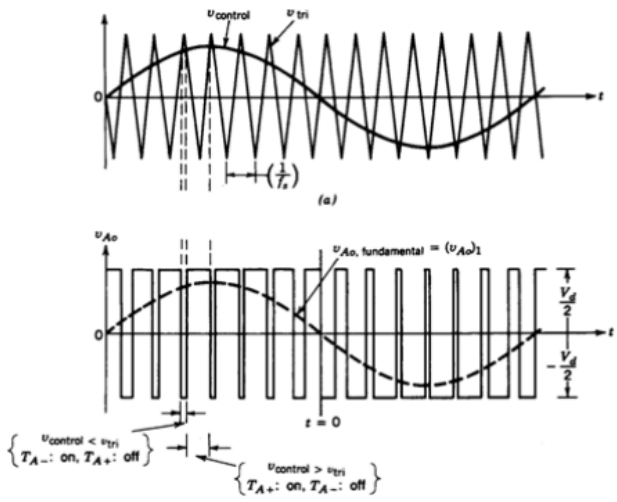

Figure C.2: Puls-width modulation[2]

The gate signals for one leg are given by comparison of a constant triangular waveform with switching frequency f_s and a sinusoidal control signal with frequency f_1. When the control signal is greater than the triangular waveform the upper switch T_{A+} in the leg are turn on, and the lower T_{A-} turned off. The two switches are never off simultaneously, and consequently it is opposite when the triangular waveform is greater than the control signal. This way the fundamental frequency off the output voltage will be f_1, and the amplitude will be dependent of the amplitude modulation ratio m_a. The amplitude modulation ratio is defined by C.1, where $\hat{V}_{control}$ are the amplitude of the control signal, and $\hat{V}_{tri}$ of the triangular waveform, also referred to as the carrier signal. [2]

$$m_a = \frac{\hat{V}_{control}}{\hat{V}_{tri}} \tag{C.1}$$

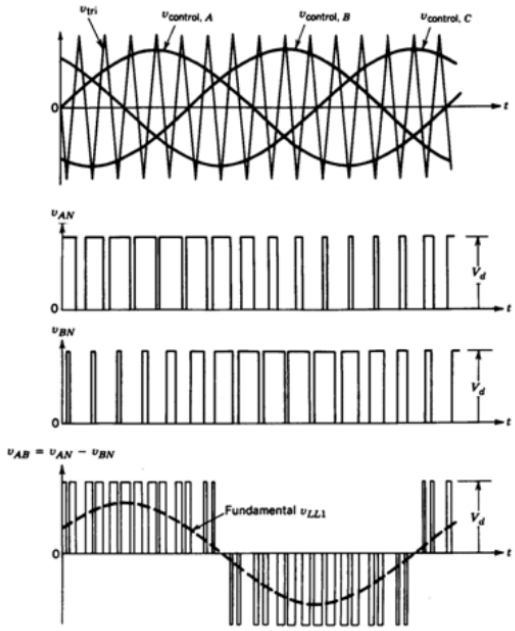

Figure C.3: Three-phase PWM waveforms

Three control signals 120°out of phase are then compared with the same carrier signal, to obtain balanced three-phase voltage at the converter terminals. The frequency and amplitude of the output voltages can therefore be controlled by regulating the control voltages. Figure C.3 shows the signals for a three-phase PWM converter, and some of the output phase and line voltages. If m_a is less than one will the converter operate in the linear region, and the fundamental component of the output voltage will vary linearly with the amplitude modulation ratio, as long as the DC link voltage V_d is kept constant. This relation is given by equation C.2. If m_a exceeds unity the converter enters the overmodulation region, where the relationship between m_a and V_{LL} is nonlinear. [2]

$$\underset{(line-line,\,rms)}{V_{LL}} = \frac{\sqrt{3}}{2\sqrt{2}} m_a V_d \simeq 0.612 m_a V_d \tag{C.2}$$